STAT1 Serotonylation Remodels CD8+ T Cell Mitochondrial Function to Potentiate Antitumor Efficacy of PD-1 Blockade

Shun Lu

shunlu@sjtu.edu.cn

Shanghai Chest Hospital, Shanghai Jiao Tong University School of Medicine https://orcid.org/0000-0001-8833-7262

Deyun MENG

Shanghai Chest Hospital, Shanghai Jiao Tong University School of Medicine

Wenqing Lu

Shanghai Chest Hospital, Shanghai Jiao Tong University School of Medicine

Chengxin Jiang

Shanghai Jiao Tong University School of Medicine

Ruiming Sun

Shanghai Chest Hospital, Shanghai Jiao Tong University School of Medicine

Ying-ying Chen

Shanghai Institute of Immunology https://orcid.org/0000-0002-1752-6119

Ping Ji

Shanghai Jiao Tong University School of Medicine

Liliang Xia

Shanghai Chest Hospital, Shanghai Jiao Tong University School of Medicine

Ying Wang

Shanghai Institute of Immunology, Department of Immunology and Microbiology, Key Laboratory of Cell Differentiation and Apoptosis of Chinese Ministry of Education https://orcid.org/0000-0003-1787-0515

Article

Keywords: 5-HT, STAT1 serotonylation, mitochondrial function, anti-PD-1 combination therapy, CD8+ T cells

Posted Date: June 30th, 2026

DOI: https://doi.org/10.21203/rs.3.rs-10006071/v1

Additional Declarations: There is **NO** Competing Interest.

STAT1 Serotonylation Remodels CD8$^+$ T Cell Mitochondrial Function to Potentiate Antitumor Efficacy of PD-1 Blockade

Deyun Meng[1†], Wenqing Lu[1†], Chengxin Jiang[2], Ruiming Sun[1], Yingying Chen[2], Ping Ji[2], Liliang Xia[1*], Ying Wang[2*], Shun Lu[1*]

[1]Shanghai Lung Cancer Center, Shanghai Key Laboratory of Thoracic Tumor Biotherapy, Shanghai Chest Hospital, Shanghai Jiao Tong University School of Medicine; Shanghai, 200030, P.R. China

[2]Shanghai Institute of Immunology, Department of Immunology and Microbiology, Key Laboratory of Cell Differentiation and Apoptosis of Chinese Ministry of Education, Shanghai Jiao Tong University School of Medicine, Shanghai, 200025, P.R. China

[*]Corresponding author. Email: shunlu@sjtu.edu.cn (S.L.); ywangssmu@shsmu.edu.cn (Y.W.); liliang-xia@sjtu.edu.cn (L.X.)

[†]These authors contributed equally to this work

Abstract

Immune checkpoint inhibitors (ICIs) have revolutionized cancer treatment, yet only a limited proportion of patients benefit from ICI monotherapy. Identifying new factors that enhance antitumor responses for combination therapy is key to improving clinical efficacy. Herein, we report that exogenous 5-HT (5-hydroxytryptamine, also named serotonin) synergizes with anti-PD-1 therapy to significantly suppress tumor growth and enhance $CD8^+$ T cell antitumor responses. Serotonylation, as a newly noted 5-HT-involved post-translational modification, is essential for T cell functionality through modulating mitochondrial function. Mechanistically, exogenous 5-HT treatment leads to STAT1 serotonylation at glutamine 285 (Q285), which is catalyzed by tissue transglutaminase 2 (TGM2) in $CD8^+$ T cells. This in turn promotes STAT1 phosphorylation at serine 727 and then represses *Mtfr2* (mitochondrial fission regulator 2) transcription to inhibit mitochondrial fission via the MTFR2-DRP1 axis, while activating *Mfn2* transcription to promote mitochondrial fusion. Clinically, higher tryptophan hydroxylase 1 (TPH1) and peripheral 5-HT levels are associated with favorable responses in patients with non-small cell lung cancer (NSCLC) receiving anti-PD-1 treatment. Together, these findings reveal a previously underappreciated serotonylation on STAT1 that remodels mitochondrial function and enhances $CD8^+$ T cell antitumor immunity. Our study raises the possibility that 5-HT supplementation may represent a potential combination strategy with ICIs in cancer immunotherapy.

Key words: 5-HT, STAT1 serotonylation, mitochondrial function, anti-PD-1 combination therapy, $CD8^+$ T cells.

Introduction

Immune checkpoint inhibitors (ICIs) have achieved remarkable clinical advancement by reinvigorating $CD8^+$ T cell-mediated anti-tumor responses in advanced or conventional therapy-resistant cancers[1-3]. However, numerous clinical studies show that although ICIs have prolonged the survival period of patients in multiple carcinomas, there show response rates of only 20%–30% to ICIs monotherapy[2,4,5]. This limited efficacy is largely attributed to T cell functional impairment within the tumor microenvironment (TME) which is driven by multiple factors. Among these factors, metabolic reprogramming is one of the key mechanisms disrupting mitochondrial function and energy production[6,7].

Mitochondrial dysfunction is characterized by structural defects, depolarization, and impaired dynamics upon chronic antigenic stimulation[8]. These abnormalities impair oxidative phosphorylation (OXPHOS), induce excessive reactive oxygen species (ROS) production and disrupt compromised bioenergetics, ultimately resulting in T cell functional defect[8-10]. Emerging evidence has also highlighted the critical role of

mitochondrial fission-fusion homeostasis in regulating T cell activation, effector function, and long-term persistence[8,10]. Although ICIs have achieved favorable clinical efficacy, many patients develop primary resistance or disease relapse, which is closed to disrupted mitochondrial dynamics in T cells[11]. In the TME, mitochondrial perturbations in $CD8^+$ T cells act as a core driver of functional decline and T cell exhaustion with transcriptional, phenotypic, and functional alterations[12]. Therefore, restoring mitochondrial homeostasis might offer a promising strategy to reverse T cell exhaustion and improve ICI therapeutic outcomes.

The emerging field of neuroimmuno-oncology underscores the pivotal role of the nervous system in shaping tumor immunity[13]. In non-neural malignancies, it is demonstrated that tumor-associated nerves including sensory nerves, parasympathetic nerves and sympathetic nerves could release multiple neurotransmitters that modulate immune cell function within the TME[14,15]. Among them, 5-hydroxytryptamine (5-HT, also named as serotonin) is abundant and exerts broad immunomodulatory effects. Notably, merely approximately 5% of systemic 5-HT is synthesized in the brain[16]. The majority of peripheral 5-HT is produced by intestinal enterochromaffin cells and subsequently stored in platelets. Its biosynthesis is catalyzed by the rate-limiting enzymes tryptophan hydroxylase 1 (TPH1) for peripheral 5-HT production and TPH2 in the nervous system. In tumor scenario, 5-HT predominantly functions as a tumor-promoting factor through three interconnected mechanisms[17]. Via 5-HT receptors, it triggers pro-survival signals (PI3K/AKT, MAPK/ERK, JAK/STAT1, Wnt/β-catenin) to promote proliferation and survival in cancer cells. It can also promote tumor angiogenesis by stimulating endothelial cell activation and elevating microvessel density. Furthermore, 5-HT suppresses anti-tumor immunity by inhibiting pro-inflammatory cytokine release and polarizing macrophages toward an M2 phenotype[18]. These mechanisms highlight that 5-HT alone acts as a pleiotropic accelerator on cell proliferation, angiogenesis, and immune escape.

Recent studies reveal that 5-HT acts on immune cells not only via receptor-mediated signaling but also through post-translational modifications (PTMs), a process termed serotonylation, in which 5-HT is covalently conjugated to target proteins via transglutaminase 2 (TGM2) catalysis—a modification initially described in neuronal and platelet biology[19-22]. Given the importance of PTMs such as glycosylation, palmitoylation and lactylation in modulating T cell function[23,24], the regulatory potential of serotonylation in $CD8^+$ T cell immunity has been recently explored. For instance, TGM2-catalyzed serotonylation of GAPDH promotes glycolysis and enhances $CD8^+$ T cell anti-tumor activity[25]. Meanwhile, autocrine signaling through 5-HT receptor further boosts T cell function[26]. Conversely, 5-HT can upregulate PD-L1 expression in tumor cells via serotonylation, thereby suppressing $CD8^+$ T cell effector functions[27]. In colorectal cancer, 5-HT promotes tumor progression via TGM2-mediated histone serotonylation in cancer-associated fibroblasts[28]. In pancreatic ductal adenocarcinoma, the histone serotonylation (H3Q5ser) remodels cellular lipid metabolism to facilitate tumor growth[29]. Intriguingly, emerging evidence reveals a more complex, context-dependent role

for 5-HT within the immune compartment. Both $CD8^+$ T cells and neuroendocrine tumor cells express a functional 5-HT metabolic machinery, comprising the synthetic enzyme TPH1, the high-affinity serotonin transporter (SERT), the catabolic enzyme monoamine oxidase A (MAOA), and the post-translational modifier TGM2[25,26,30,31]. These comprehensive findings reflect the dual and highly context-dependent role of 5-HT in anti-tumor immunity, revealing a critical knowledge gap that demands deeper mechanistic exploration.

In this study, we have observed that exogenous 5-HT supplementation significantly reduced tumor growth and enhanced the antitumor activity of $CD8^+$ T cells when co-administered with anti-PD-1 antibody. Further experiments demonstrated that TGM2-dependent serotonylation of signal transducer and activator of transcription (STAT1) promoted $CD8^+$ T cell functions. Gln285 of STAT1 was identified as the serotonylation site, which facilitated the transcription of mitochondrial fission regulator 2 (MTFR2) and mitochondrial functionality. Our findings thus unveil a serotonylation-mitochondria axis in modulating $CD8^+$ T cell function, offering a translational strategy to enhance ICI therapy by targeting serotonylation.

Results

Exogenous 5-HT synergizes with anti-PD-1 to suppress tumor growth

To explore the potential roles of 5-HT in tumor progression, mice bearing subcutaneous lung cancer cell line SJT1601 were subjected to intravenous administration of PBS, anti-PD-1 monoclonal antibodies (αPD-1), 5-HT, and the combination of 5-HT and αPD-1 (5-HT+αPD-1) (Fig. 1a). It was found that high levels of serum 5-HT were detectable in 5-HT fed mice (Extended Data Fig. 1a). Moreover, tumor growth was significantly slowed down, and tumor weight was reduced in the 5-HT-treated mice as compared to the PBS-treated mice. Notably, the combined treatment of 5-HT and αPD-1 displayed the best anti-tumor efficacy, as evidenced by the smallest tumor size and lowest tumor weight in the SJT1601 tumor-bearing mice (Fig. 1b, c and Extended Data Fig. 1b). In the 5-HT+αPD-1 group, we observed increased production of IFNγ and GzmB in tumor-infiltrating $CD8^+$ T cells (Fig. 1d). In addition, the expression of exhaustion markers including KLRG1 and LAG3 in $CD8^+$ T cells was significantly reduced as compared to other three groups (Extended Data Fig. 1c). However, the percentages of natural killer (NK) cells and the production of IFNγ, TNFα and GzmB in NK cells remained comparable among all groups (Extended Data Fig. 1d). Given that tumor-specific memory $CD8^+$ T cells are bona fide responders to PD-1/PD-L1 blockade in draining lymph nodes[32], we observed greatly increased $CD44^+CD62L^+$Tcm-like cells in tumor dLNs (TdLNs) from 5-HT+αPD-1 group mice (Extended Data Fig. 1e). We further sorted $CD8^+$ T cells from the TdLNs of tumor-bearing mice and stimulated with αCD3/αCD28 *in vitro*. $CD8^+$ T cells were then co-cultured with tumor cells. It was obvious that $CD8^+$ T cells from 5-HT+αPD-1 combination therapy group mice exhibited

the strongest cytotoxic activity among four groups (Extended Data Fig. 1f). Similarly, combined treatment of 5-HT and αPD-1 significantly delayed tumor growth with reduced tumor weight in MC38-grafted mice (Fig. 1e-h and Extended Data Fig. 1g). Production of IFNγ and GzmB in $CD8^+$ T cells was elevated the most dramatically as well in mice receiving combination treatment when compared to other three treatments (Fig. 1h).

To determine whether $CD8^+$ T cells are involved in tumor suppression upon 5-HT+αPD-1 combination treatment, we depleted $CD8^+$ T cells with an anti-mouse CD8 monoclonal antibody (mAb) in SJT1601-bearing mice (Fig. 1i). We found that $CD8^+$ T cell depletion abrogated the suppression on tumor growth observed in 5-HT+αPD-1 group. Tumor growth and tumor weight were similar to those in αPD-1 or 5-HT groups (Fig. 1j-k). Similarly, $CD8^+$ T cell depletion led to the reverse of tumor growth and weight in 5-HT+αPD-1 treated group mice that was comparable to αPD-1 or 5-HT single treatment in MC38-grafted mice (Fig. 1l-n). These results demonstrate that 5-HT synergizes anti-tumor efficacy of anti-PD-1 treatment in tumor-grafted mice predominantly in a $CD8^+$ T cell dependent manner.

Serotonylation is indispensable for $CD8^+$ T cell antitumor function upon 5-HT supplementation

Although we have observed elevated 5-HT levels in the periphery of 5-HT supplemented mice, the underlying mechanisms of enhanced $CD8^+$T cell functionality in 5-HT supplemented tumor-bearing mice need to be further investigated. We firstly determined the distribution of 5-HT in tumor regions. By flow cytometric analysis on tumor infiltrating $CD8^+$ cells it was showed that both αPD-1 and 5-HT treatment alone elevated 5-HT levels in $CD8^+$ T cells while combination treatment resulted in a more significant increase (Fig. 2a). αPD-1-induced 5-HT elevation in $CD8^+$T cells was also confirmed by immunofluorescence assays on tumor tissues (Fig. 2b and Extended Data Fig. 2a). When we stimulated $CD8^+$ T cells with αCD3/αCD28 *in vitro*, we not only observed the accumulation of intracellular 5-HT and secretion of 5-HT to the culture supernatant (Fig. 2c, d), serotonylation level was also dramatically increased in $CD8^+$ T cells upon αCD3/αCD28 stimulation (Fig. 2e and Extended Data Fig. 2b).

TGM2 is a key enzyme that is expressed in $CD8^+$ T cells and catalyzed the serotonylation reaction through transferring 5-HT to the Gln residues of target proteins[25]. To elucidate the roles of serotonylation in $CD8^+$ T cell anti-tumor immunity, we added LDN27219, a specific TGM2 inhibitor to *in vitro* $CD8^+$ T cell activation system. It was shown that LDN27219 treatment inhibited T cell proliferation (Fig. 2f) and reduced the proportions of CD107a, GzmB, IFNγ and TNFα-secreting $CD8^+$ T cells (Fig. 2g), which is similar to the results from *tgm2*-deficient $CD8^+$ T cells[25]. Functional enrichment analysis revealed that LDN27219 impaired immune response functions (Extended Data Fig. 2c). GSEA analysis also showed impaired cytokine activity in LDN27219-treated T cells (Extended Data Fig. 2d).

To further validate the putative role of serotonylation in regulating $CD8^+$ T cell function during anti-PD-1 treatment, we adoptively transferred $CD8^+$ T cells from *Tgm2*$^{-/-}$ and wild-type (WT) mice into *Rag1*$^{-/-}$ mice and monitored *in vivo* tumor growth of SJT1601 (Fig. 2h). Mice reconstituted with *Tgm2*$^{-/-}$ $CD8^+$ T cells exhibited significantly larger tumor volumes and heavier tumor weight than those receiving WT $CD8^+$ T cells (Fig. 2i, j). Consistently, the percentages of IFNγ- and GzmB-producing tumor-infiltrating $CD8^+$ T cells were significantly reduced in *Rag1*$^{-/-}$ mice reconstituted with *Tgm2*$^{-/-}$ $CD8^+$ T cells (Fig. 2k). There results demonstrate that serotonylation promotes $CD8^+$ T cell effector function both *in vitro* and *in vivo*.

Inhibition of serotonylation in $CD8^+$ T cells dampens mitochondrial function

Next, we explored the mechanism of how serotonylation regulating $CD8^+$ T cell functionality. GSEA analysis showed that ROS-related genes were significantly enriched in LDN27219-treated $CD8^+$ cells when compared to control $CD8^+$ T cells (Fig. 3a). We further evaluated mitochondrial membrane potential (MMP) and mitochondrial ROS (mtROS) levels by staining cells with MitoTracker dye, TMRM, and MitoSOX respectively. It was shown that LDN27219-treated $CD8^+$ T cells exhibited significantly elevated MMP and mtROS, indicating excessive mitochondrial activation accompanied by high MMP and increased oxidative stress (Fig. 3b). Furthermore, transmission electron microscope revealed that LDN27219 treatment reduced both the number and area of mitochondria (Fig. 3c). LDN27219-treated $CD8^+$ T cells also displayed a significantly lower mitochondrial oxygen consumption rate (OCR) with reduced spare respiratory capacity compared to control cells, along with a slight reduction in the extracellular acidification rate (ECAR) (Fig. 3d and Extended Data Fig.3a, b). Consistent with these metabolic defects, C12-resazurin staining confirmed a significant reduction in the metabolic activity of $CD8^+$ T cells following LDN27219 treatment (Fig. 3e). Intracellular ATP content was also reduced in LDN27219-treated $CD8^+$ T cells compared to control cells (Fig. 3f). These results demonstrate that serotonylation is involved in maintaining mitochondria metabolic activity and effector function in $CD8^+$ T cells.

Serotonylation at Gln285 of STAT1 facilitates mitochondrial function

To identify serotonylated proteins in $CD8^+$ T cells, we performed immunoprecipitation (IP) by using an anti-5-HT antibody in both resting and anti-CD3/CD28 activated $CD8^+$ T cells, followed by targeted liquid chromatography-tandem mass spectrometry (LC-MS/MS) (Fig. 4a). In total, 589 proteins were identified at the 0 h time point and 1014 proteins at 48 h. Among these candidates, 483 proteins were detected at both time points, whereas 531 proteins were exclusively identified at 48 h post activation (Fig. 4b). Gene Ontology (GO) enrichment analysis was performed on proteins exhibiting >2-fold changes (48 h vs. 0 h) as well as those uniquely detected at 48 h. The results revealed significant enrichment in categories including mitochondrial protein complexes and ATP-dependent protein folding chaperones (Fig. 4c). Following

extensive screening by immunoprecipitation and Western blot, STAT1 was detected in 5-HT antibody immunoprecipitates from WT $CD8^+$ T cells, but not from *Tph1*$^{-/-}$ $CD8^+$ T cells (Fig. 4d). Conversely, 5-HT was detected in STAT1 antibody immunoprecipitates (Fig. 4e). These findings indicate that STAT1 is one of the serotonylated target proteins in activated $CD8^+$ T cells. To further assess whether STAT1 is a direct substrate for serotonylation, we conducted an *in vitro* enzymatic assay by using recombinant TGM2 and monodansylcadaverine (MDC), a fluorescent monoamine analog. Fibrinogen is a previously well-established serotonylation substrate and used as a positive control in the reaction. The results showed that robust MDC incorporation was observed in STAT1, confirming the presence of TGM2-induced transamidation reaction on STAT1 (Fig. 4f).

To map the serotonylation sites on STAT1, we performed LC-MS/MS analysis on the samples from *in vitro* TGM2 enzymatic assays with MDC labeling. Tandem mass spectrometry identified two glutamine residues, Gln120 and Gln285, as potential serotonylation sites in recombinant human STAT1 (Fig. 4g and Extended Data Fig. 4a). Given the high sequence conservation of STAT1 across species (Fig. 4h), we synthesized short mouse peptides encompassing Q120 and Q285 and subjected them to *in vitro* TGM2 enzymatic reactions. Peptide-level mass spectrometry validated both Gln120 and Gln285 as bona fide serotonylation substrates, as evidenced by successful MDC and 5-HT conjugation modifications (Fig. 4i-j and Extended Data Fig. 4b, c).

To further dissect the functional roles of STAT1 serotonylation at these two sites, we constructed lentiviral vectors encoding wild-type STAT1 (WT-STAT1) or STAT1 Gln-to-Ala point mutants (Q120A and Q285A) and transduced them into murine EL4 T lymphoma cells, transfection efficiency was detected by flow cytometry (Extended Data Fig. 4d). Following stimulation with anti-CD3/anti-CD28 antibodies in the presence or absence of 5-HT, we evaluated mitochondrial function across all groups. We found that the Q285A, but not Q120A, mutation markedly elevated mitochondrial membrane potential (MMP) and mtROS levels under both conditions (Fig. 4k). Consistently, C12-resazurin staining revealed substantially reduced cellular metabolic activity specifically in Q285A-mutant EL4 cells but not in the Q120A mutant (Fig. 4l). Similarly, ATP production was inhibited in Q285A-STAT1-mutated EL4 cells but not in the Q120A mutant (Fig. 4m). Transmission electron microscopy (TEM) further confirmed that the Q285A mutation led to a notable reduction in mitochondrial abundance (Fig. 4n-o). Collectively, these results demonstrate that STAT1 serotonylation at Q285 is a novel post-translational modification that sustains mitochondrial function in T cells.

STAT1 serotonylation modulates mitochondrial function through enhancing STAT1 S727 phosphorylation

To investigate whether STAT1 itself functionally contributes to the serotonylation-associated phenotypes, we treated $CD8^+$ T cells with fludarabine, a specific STAT1 inhibitor. Fludarabine treatment led to phenotypes similar to those observed upon serotonylation inhibition (Fig. 3b). it elevated mitochondrial markers (Mitotracker, TMRM, mtROS), impaired ATP production, reduced effector molecule expression (CD107a, IFN-γ, TNF-α) in a dose-dependent manner (Extended Data Fig. 5a-c), and exacerbated $CD8^+$ T cell exhaustion with impaired antitumor function (Extended Data Fig. 5d-f). Thus, STAT1 is not only a substrate for serotonylation but also functionally required for maintaining mitochondrial function and $CD8^+$ T cell activity, prompting us to further dissect how its serotonylation regulates these processes.

We further investigated how STAT1 serotonylation modulates mitochondrial homeostasis. In line with a previous report[33], αCD3/αCD28 stimulation induced STAT1 phosphorylation specifically at Ser727 (S727) site, but not at Tyr701 site, in $CD8^+$ T cells, and this S727 phosphorylation was completely abrogated by PP2, an inhibitor of Src family kinase (Extended Data Fig. 6a), indicating that S727 is a key functional phosphorylation site downstream of TCR signaling. We thus hypothesized that STAT1 serotonylation might regulate its S727 phosphorylation. As shown in Fig 5a, the levels of $pSTAT1^{S727}$ were elevated in freshly isolated TdLN $CD8^+$ T cells from 5-HT-treated SJT1601 tumor-bearing mice. Conversely, treatment with LDN27219 suppressed $pSTAT1^{S727}$ levels in anti-CD3/CD28 activated $CD8^+$ T cells *in vitro*, accompanied by increased DRP1 and decreased MFN2 expression (Fig. 5b), suggesting enhanced mitochondrial fission and reduced fusion upon impaired serotonylation. Consistently, the STAT1 Q285A mutant abolished 5-HT-induced $pSTAT1^{S727}$ elevation in transfected EL4 cells (Fig. 5c). Futhermore, LDN27219 treatment suppressed *Mfn2* mRNA expression while upregulating *Mtfr2* (mitochondrial fission regulator 2), with no significant change in *Dnm1l* (encoding DRP1) mRNA levels (Fig. 5d and Extended Data Fig. 6b). Similar results were obtained with fludarabine. Together, these results demonstrate that STAT1 serotonylation at Q285 promotes STAT1 S727 phosphorylation.

STAT1 is primarily recognized as a transcription factor that regulates both innate and adaptive immunity. To explore whether $pSTAT1^{S727}$ directly controls the expression of mitochondrial dynamic-related genes, we analyzed ChIP-seq data from human SET-2 cells using an antibody specific for STAT1 phosphorylated at Ser727. This analysis identified peaks in the promoter regions of *MFN2* and *MTFR2* (Extended Data Fig. 6c, 6d). Moreover, integration with H3K27ac ChIP-seq data indicated that these peak regions are lie within active chromatin domains (Extended Data Fig. 6c, 6d). To validate this in the mouse system, we performed ChIP using an anti-$pSTAT1^{S727}$ antibody in activated mouse $CD8^+$ T cells, and qPCR validation confirmed that $pSTAT1^{S727}$ binds to the promoters of *Mfn2* and *Mtfr2*. Notably, while $pSTAT1^{S727}$ occupancy correlated with increased *Mfn2* expression, it inversely correlated with *Mtfr2* expression (Fig. 5d), suggesting that

pSTAT1^{S727} differentially regulates these two targets, acting as an activator for *Mfn2* and a repressor for *Mtfr2*.

It has been reported that MTFR2 protein binds to DRP1, preventing its lysosomal degradation and thereby promoting mitochondrial fission[34]. To confirm the MTFR2-DRP1 interaction, we transduced El4 cells with mCherry-fused lentiviruses carrying a FLAG-tagged *mtfr2* construct. Co-immunoprecipitation with an anti-FLAG antibody successfully pulled down DRP1 (Fig. 5f), and immunofluorescence staining revealed not only elevated DRP1 expression in MTFR2-overexpressing cells but also co-localization of MTFR2 and DRP1 (Fig. 5g). Consistent with these observations, siRNA-mediated knockdown of *Mtfr2* in EL4 cells (Extended Data Fig. 6e) suppressed both phosphorylated and total DRP1 protein levels while increasing MFN2 expression (Fig. 5h), indicating a shift toward enhanced mitochondrial fusion and reduced fission Accordingly, *Mtfr2* interference led to a decrease in mitochondrial numbers (Fig. 5i).

Together, these findings establish that serotonylation of STAT1 at Q285 promotes its S727 phosphorylation. This phosphorylated STAT1 then acts as a dual regulator. On one hand, it represses *Mtfr2* transcription, reducing MTFR2 protein and thereby relieving DRP1 from MTFR2-mediated stabilization, which inhibits mitochondrial fission. On the other hand, it activates Mfn2 transcription to promote mitochondrial fusion. Thus, STAT1 serotonylation coordinates both fission and fusion programs to modulate mitochondrial homeostasis in CD8$^+$ T cells.

Clinical relevance of 5-HT in anti-PD-1 therapy

To explore the clinical relevance of 5-HT in anti-tumor immunity, we analyzed public single-cell RNA-seq data from human tumor samples (GSE189357). TPH1, the rate-limiting enzyme for 5-HT synthesis, was broadly expressed across multiple cell types but at very low levels (Extended Data Fig. 7a-b). Given interpatient variability, samples were stratified into TPH1_high and TPH1_low groups (Extended Data Fig. 7c). Unsupervised clustering identified six CD8$^+$ T cell subsets (Extended Data Fig. 7d). The TPH1_high group showed significantly higher proportions of tissue-resident memory (TRM) and central memory CD8$^+$ T cells (Fig. 6a) lower exhaustion scores (Fig. 6b), and reduced PD-1 expression in terminal effector CD8+ T cells (Fig. 6c). These human data align with our mouse model findings, suggesting that elevated 5-HT (indicated by TPH1 expression) associates with a low-exhaustion state in CD8$^+$ T cells, potentially more responsive to anti-PD-1 immunotherapy.

We next analyzed a separate single-cell dataset from NSCLC patients receiving anti-PD-1 plus chemotherapy (GSE207422; pre-treatment n=3, post-treatment non-responders [NR] n=8, responders [R] n=4) (Extended Data Fig. 7e). Post-treatment, both NR and R groups showed increased T cells and plasma cells and decreased neutrophils and myeloid cells, with more pronounced changes in responders (Fig. 6d). At

the bulk level, the increase in TPH1$^+$ T cells from 33% (pre) to 100% post-treatment is striking, but due to limited sample size the Kruskal-Wallis test was not significant (p = 0.052) (Fig. 6e). Nevertheless, this trend suggests a potential link between 5-HT and therapy exposure, motivating us to further examine 5-HT levels in patient sera.

To further investigate the relationship between 5-HT and treatment response, we next assessed serum 5-HT levels in 46 patients with advanced non-small cell lung cancer (NSCLC) receiving nivolumab (anti-PD-1) therapy (Table 1), measured at baseline and four weeks after the first treatment (Fig. 6f). At the first evaluation, 24 patients achieving partial response or stable disease were classified as responders, while 22 patients with progressive disease were classified as non-responders. No significant difference in baseline 5-HT levels were observed between responders and non-responders. After treatment, 5-HT levels were significantly elevated from baseline in responders, but not in non-responders (Fig. 6g). Pearson correlation analysis revealed a statistically significant positive association between 5-HT levels and progression-free survival (PFS) (R=0.4071 p=0.0041), indicating that higher 5-HT levels correlated with longer PFS (Fig. 6h). Furthermore, a significant negative correlation was observed between the proportion of LAG3$^+$ CD8$^+$ T cells in peripheral blood and 5-HT levels (R=-0.5129, p=0.0016), suggesting a moderate inverse relationship (Fig. 6i). Collectively, these human single-cell and serum clinical data are broadly consistent with our mouse mechanistic findings and raise the possibility that higher 5-HT levels may be favorable for improving the clinical response to anti-PD-1 therapy.

Discussion

In this study, we identified serotonylation as a novel post-translational modification of STAT1 that promotes its phosphorylation at Ser727, thereby influencing T cell function through the transcriptional regulation of mitochondrial-related proteins.

It is well established that the transcriptional activity of STAT1 requires coordinated phosphorylation at two key residues: tyrosine 701 (Y701), which enables DNA binding, and serine 727 (S727), which enhances transcriptional activation[33]. While Y701 phosphorylation is primarily mediated by the canonical JAK/STAT pathway[35], S727 phosphorylation exhibits cell type- and stimulus-specificity. In human T cells, TCR signaling stimulates S727, but not Y701, phosphorylation of STAT1, and the Src family kinase inhibitor PP1 completely abrogated CD3-mediated S727 phosphorylation[33]. In mouse CD8$^+$ T cells, we confirmed that CD3/CD28 induces S727 phosphorylation of STAT1, which is abrogated by the Src family kinase inhibitor PP2 (Extended Data Fig. 6a).

Current evidence indicates that STAT1 predominantly exerts indirect effects on mitochondrial function, primarily through three mechanisms: (i) transcriptional regulation of apoptosis-associated genes[36], (ii)

functional interplay with other STAT family members (e.g., STAT3)[37,38], and (iii) modulation of mitochondrial metabolic pathways via intermediary regulatory factors[39,40]. However, conclusive evidence substantiating direct mitochondrial localization of STAT1 or its immediate regulation of mitochondrial protein expression remains absent.

It is worth noting that the dual regulatory capacity of pSTAT1^{S727}—exerting opposing effects on different target genes—is not without precedent. In the context of IFN-γ signaling, Bancerek and colleagues demonstrated that CDK8-mediated STAT1 S727 phosphorylation positively or negatively regulates over 40% of IFN-γ-responsive genes, a divergent regulation that occurs despite comparable CDK8 occupancy at both up- and down-regulated targets[41,42]. Thus, the ability of pSTAT1^{S727} to act as both an activator and a repressor is an inherent property of the STAT1 transcription factor, likely dictated by the chromatin context and co-regulatory partners at individual promoters. Extending this concept, we show here that in activated CD8$^+$ T cells, pSTAT1^{S727} directly binds to the promoters of *Mfn2* and *Mtfr2* but exerts opposite effects on their transcription: activating *Mfn2* to promote mitochondrial fusion while repressing *Mtfr2* to suppress MTFR2-mediated DRP1 stabilization and fission. Together, these findings establish STAT1 S727 phosphorylation as a key node that integrates upstream signaling inputs (serotonylation) to coordinate bidirectional control of the mitochondrial dynamics network.

Through targeted mass spectrometry and amino acid mutagenesis, we identified Q285 as the site of STAT1 serotonylation within its coiled-coil domain (CCD). STATs use this domain for dimerization and/or interactions with other transcription factors or regulatory proteins, thereby influencing the transcriptional activity of downstream genes[35,43,44]. In a recently characterized post-translational modification, vitcylation of K298 disrupts the anti-parallel conformation of pSTAT1, a conformation essential for binding to T cell protein-tyrosine phosphatase (TCPTP) and subsequent dephosphorylation, thereby elevating pSTAT1 levels and enhancing IFN-mediated immune responses[45]. Given that both K298 and Q285 reside within the CCD, the serotonylation of Q285 may regulate STAT1 phosphorylation and transcriptional activity through a mechanism analogous to that of K298 vitcylation.

This study identifies serotonylation as a unique post-translational modification that integrates neurotransmitter signaling (5-HT) with T cell metabolism via STAT1. Unlike classical STAT1 phosphorylation pathways, serotonylation operates through TGM2-mediated protein modification, expanding the toolkit for metabolic immune regulation. The discovery of MFN2 and MTFR2 as STAT1 target genes further links mitochondrial dynamics to T cell function.

Extending our mechanistic findings to the clinical setting, we analyzed human single-cell RNA sequencing data from NSCLC patients and found that TPH1_high tumors are characterized by CD8$^+$ T cells with lower exhaustion scores. In a cohort of 46 advanced NSCLC patients receiving nivolumab, higher serum 5-HT

levels correlated with longer progression-free survival and negatively correlated with the proportion of $Lag3^+$ $CD8^+$ T cells. In an independent cohort of NSCLC patients receiving anti-PD-1 plus chemotherapy, *TPH1* expression in T cells increased following treatment, with particularly striking elevations in responders. These clinical data are broadly consistent with our mechanistic findings in mice and suggest that higher 5-HT levels may be favorable for improving responses to anti-PD-1 therapy.

ICIs have revolutionized cancer therapy, yet a significant proportion of patients fail to respond to monotherapy due to tumor immune evasion mechanisms[1]. Identifying novel factors that enhance antitumor immunity and enable effective combination strategies is critical to improving clinical outcomes. Here, we demonstrate that extracellular 5-HT synergizes with anti-PD-1 therapy to suppress tumor growth and enhance $CD8^+$ T cell function through serotonylation-mediated mitochondrial remodeling. We have uncovered a previously unknown role of serotonylation in T cell metabolism, providing a strong rationale for targeting this pathway alongside ICIs in cancer therapy.

Limitation of the study

Several limitations of this study should be acknowledged. First, prior research has shown that serotonylation occurs as a post-translational modification in a wide range of proteins. Our LC-MS/MS-based proteomic analysis detected hundreds of potential serotonylated proteins in $CD8^+$ T cells. It remains possible that additional serotonylated proteins contribute to T cell function. Second, our data indicate that anti-PD-1 antibody treatment increases intracellular 5-HT levels in T cells. However, the precise mechanism is not yet understood and may involve modulation by different functional states of the cells. Further research is needed to elucidate this mechanism. Third, the human single-cell analyses were based on publicly available datasets with relatively small sample sizes, and the serum 5-HT measurements were performed in a single-center cohort without an independent external validation. Fourth, causality between 5-HT elevation and treatment response cannot be firmly established from correlative clinical data. Prospective clinical studies with larger sample sizes are warranted to validate the biomarker potential of 5-HT and to determine whether exogenous 5-HT could improve immunotherapy outcomes.

Acknowledgements

This study was supported by the National Postdoctoral Researcher Program of China GZC20231628 (to D.Y.M), the National Natural Science Foundation of China (32300763 to D.Y.M, 82030045 to S.L, 92478203 to L.L.X), Collaborative Innovation Center for Clinical and Translational Science by Ministry of Education & Shanghai (CCTS-202407PT and CCTS-202508PT to S.L), Shanghai Chest Hospital Basic Research Project (2023YNKT-1 to S.L), Shanghai Key Laboratory of Thoracic Tumor Biotherapy (2025SZ1710 to S.L), and Shanghai Health Commission Leading Talent Project (2022LJ016 to Y.W). We

thank all lab members for helpful discussions. We also appreciate the Animal Center and all technology platforms for their essential technical assistance.

Author contributions

D.M. designed and performed experiments, analyzed data, and wrote the manuscript. W.L. designed and performed in vivo experiments, and collected patient samples and clinical information. C.J. provided technical support for bioinformatics analysis. R.S. provided technical support for in vivo experiments. Y.C. and P.J. discussed and interpreted the data. L.X., Y.W., and S.L. conceived and supervised the project, and edited the manuscript. All authors contributed to the manuscript preparation. D.M is the guarantor of this work and has full access to all the data in the study.

Declaration of interests

The authors declare no competing interest.

Methods

Experimental model and subject details

Mice

All mice were housed in a specific-pathogen-free environment with a 12h light/light cycles and with controlled temperature 23-25ºC. 6-8 weeks old C57BL/6 were purchased from shanghai lingchang Biotechnology Co., Ltd (China). *Tgm2*$^{-/-}$ (Cat. NO. NM-KO-191051) and *Rag1*$^{-/-}$ (Cat. NO. NM-KI-00069) mice were purchased from Shanghai Model Organisms Center, Inc.(China). All mice were used in accordance with protocols approved by the Institutional Animal Care and Use Committee (IACUC) of Shanghai Jiao Tong University School of Medicine.

Cells and cell culture

All cells were cultured under an atmosphere of 5% CO_2 at 37 ºC. The SJT1601 cell line of mouse lung adenocarcinoma cells (donated by Dr. Jiong Deng from Shanghai Jiaotong university School of Medicine), the MC38 cell line (previously purchased from the Shanghai Institute of Biochemistry and Cell Biology, China) and the EL4 cell line (purchased from Shanghai Fuheng Biotechnology Co.,Ltd. China) were all cultured in complete Dulbecco's Modified Eagle Medium (DMEM, Thermo) containing 10% fetal bovine serum (FBS, Gemini) and 1% penicillin/streptomycin (Thermo). Mouse primary $CD8^+$ T cells were cultured in RPMI 1640 (Thermo) supplemented with 10% FBS (GIBCO), penicillin/streptomycin, L-glutamine (4 mM; Thermo), 2-mercaptoerhanol (50 mM; Sigma), HEPES (10 mM; Thermo) and non-essential amino acids (Thermo).

Human subjects

This study enrolled patients with advanced non-small cell lung cancer (NSCLC) were participants in the clinical trial CheckMate870 (NCT03195491) conducted at Shanghai Chest Hospital, affiliated with Shanghai Jiao Tong University School of Medicine. As described in our previously published article[46], this study enrolled advanced IIIB/IV NSCLC patients who progressed after 1–2 prior systemic therapies, assessed measurable disease via CT/MRI per RECIST 1.1, and treated them with intravenous nivolumab (3 mg/kg every two weeks) until progression or unacceptable toxicity, with response evaluation every six weeks (confirmation $\geqslant$ 4 weeks after initial response) and classification as responders [progression-free survival (PFS) >180 days] or non-responders (PFS <180 days) based on Response Evaluation Criteria in Solid Tumors version 1.1 (RECIST 1.1). All patients were informed of the study and consented to the enrollment. The study was approved by the Ethics Committee of Shanghai Chest Hospital (Approval ID: KS21005). Key patient attributes for the NSCLC cohort are detailed in Table 1.

Method details

Mouse tumor models

Tumor cells were subcutaneously inoculated into the right axillary region of 8-week-old mice (10^6 SJT1601 cells or 5×10^5 MC38 cells per mouse). Tumor length and width were measured every 2-3 days to calculate tumor volume (=length × $width^2$ × 0.5). For the extra 5-HT supplementation groups, 200 μg/100 μl 5-HT (Sigma, H9523) were intraperitoneally (i.p.) injected per mouse from tumor inoculation every other day. For anti-PD-1 therapy, 100 μg/100 μl mouse anti-PD-1 monoclonal antibodies (clone RMP1-14, BioXCell) were i.p. injected on day 10, 13 and 16 in SJT1601-implanted mice and 200 μg/100 μl anti-PD-1 monoclonal antibodies were i.p. injected on day 7, 10 and 13 in MC38-implanted mice after tumor cell inoculation (day 0). For depletion of $CD8^+$ T cells, 200 μg/100 μl anti-CD8 monoclonal antibodies (clone 2.43, BioXCell) were injected i.p. at day -2, 5 and 12. For *Rag1*$^{-/-}$ adoptive transfer experiments, 10^7 purified $CD8^+$ T cells from lymph nodes and spleen of WT or *Tgm2*$^{-/-}$ mice were intravenously (i.v.) injected 2 days before SJT1601inoculation. Mice were sacrificed at the indicated time points, and tumor weight was measured.

Preparation of mouse tumor infiltrating lymphocytes

Tumor tissues were minced into small pieces, and resuspended in DMEM medium with 0.5mg/mL Collagenases II, 0.5mg/mL Collagenases IV and 0.1mg/mL DNase I (StemCell, 07426, 07418 and 07470), followed by digestion for 30 minutes in a 37ºC incubator. Cell suspensions were sequentially filtered through 70-mm cell strainers to isolate single-cell suspensions.

In vitro murine CD8$^+$ T cells experiments

CD8$^+$ T cells for in vitro experiments were isolated from the spleens and lymph nodes of mice using the Mouse CD8$^+$ T Cell Isolation Kit (StemCell,19853) following the manufacturer's protocol. The purity was validated at >95% via flow cytometric analysis. Purified CD8$^+$ T cells or EL4 cells were cultured in plates pre-coated with 2 μg/mL αCD3/αCD28 (Thermo, 16-0031-38, 26-0281-86) in complete RPMI 1640 medium as described before for 24-72 h. 10 ng/mL recombinant mouse IL-2 (ABclonal, RP01384) was involved in all CD8$^+$ T cell cultures except in memory-induced experiments. For proliferation studies, CD8$^+$ T cells were labelled with 5 μM CFSE (invitrogen) and then activated with αCD3/αCD28 with or without 50 μM TGM2 inhibitor LDN27219 for 72 h. The proliferation of CD8$^+$ T cells was detected by flow cytometry and analyzed by CFSE dilution. For CD8$^+$ T cells function analysis, cells were harvested at 48 h post-stimulation and cultured with protein transport inhibitor GolgiStop (BD) for 4 hours prior to further flow cytometry staining. To induce T cell exhaustion in vitro, CD8$^+$ T cells were initially activated for 3 days via αCD3/αCD28 stimulation, followed by another 3 days of activation on plates, and then subjected to flow cytometry staining. For assessment of mitochondrial function, cells were harvested at 24 h post-stimulation and stained with surface marker CD8 and live/dead dye (Thermo), and then stained with 1 μM Mitotracker, TMRM (1:1000), 5 μM mitoSOX (Thermo; M22426, M36008, 134361) in 37ºC for 30 min followed by cleaning and analyzed with flow cytometry within one hour. For Metabolic activity was determined using a Vybrant Cell Metabolic Assay Kit (containing C12-resazurin) (Thermo, V23110), In a 96-well plate, activated cells were incubated with 10 μM C12-resazurin at 37°C for 15 min. Fluorescence was measured by flow cytometry. For inhibition experiments, 50 μM LDN27219 and 10 μM Fludarabine (MedChemExpress; HY-16693, HY-B0069) were used during CD8$^+$ T cell stimulation.

Flow cytometry

For surface staining, cells were stained with a Fixable viability dye and surface marker in PBS containing 2% FBS. For interacelluar cytokine detection, cells were stimulated with phorbol 12-myristate 13-acetate (PMA, 100 ng/mL, Sigma-Aldrich), ionomycin (1 mg/mL, Sigma-Aldrich) and GolgiStop (0.1%, BD Biosciences) for 4 h.

For in vitro CD8$^+$ T cell cytokine detection, only 0.1% GolgiStop^{TM} were added to the culture medium before staining for 4 h. Cells were subjected to intracellular staining using a Cytofix/Cytoperm^{TM} Kit (BD Biosciences) following the manufacturer's instructions. Cells were subjected to intracellular staining using a Cell Fixation/Permeabilization Kit (BD Biosciences) following the manufacturer's instructions. Stained cells were analyzed using BD LSRFortessa x20 Flow Cytometer (BD Biosciences). FlowJo 10 software (Tree Star) was used to analyze the data.

Immunofluorescence analysis

Fresh tumor tissues were fixed with in Universal Tissue Fixative (Servicebio) for more than 24 h. The tissues were then embedded in paraffin after dehydration, clearing and infiltration according to routine procedures. Tissue section (8-10 μm) were prepared from the paraffin-embedded tumor samples and subjected to immunofluorescence assay. Briefly, the slides were preformed standard dewaxing and rehydration and tissue antigen retrieval with sodium citrate under high temperature and high pressure. Then donkey and mouse serum were added to the slides to block non-specific binding for 30 min and anti-5-HT goat antibody (1:400, ab66047, Abcam) and anti-CD8a rabbit antibody (1:500) were incubated with tissues at 4ºC overnight. The slides were rinsed three times with TBS and incubated with AF488-mouse anti-rabbit (1:800), AF594-donkey anti-Goat (1:800) at room temperature for 1 hour in dark. The slides were washed three times with TBS. DAPI solution (1:500) was added for nuclear labeling with 10 min dark incubation. The slides were mounted using vectashield mounting media and were imaged using Olympus SLIDEVIEW^{TM} VS200 Research Slide Scanner.

Extracellular flux analysis

Oxygen consumption rate (OCR) and Extracellular acidification rate (ECAR) were separately measured by the Seahorse XF analyzer with Mitochondrial stress test (MST) and Glycolysis Stress Test (GST) (Agilent Technologies, 103015-100, 103020-100) according to the manufacturer's instructions. Briefly, $2x10^5$ activated T cells were plated in Cell-Tak-coated XF96 plates in RPMI medium in the presence of the following compounds: 2 μM oligomycin, 1 μM FCCP, and 0.5 μM rotenone/antimycin A for OCR, and 50 μM 2-DG, 10 mM glucose, and 2 μM oligomycin for ECAR (Agilent Technologies).

Transmission electron microscopy (TEM) experiment

Activated $CD8^+$ T cells in present or absent of LDN27219, and EL4 cells cultured with 5-HT and αCD3/αCD28 for 24 h, were fixed in fresh electron microscope fixative (2.5% glutaraldehyde, Biossci) followed by secondary fixation with 1% osmium tetroxide to stabilize lipids and enhance contrast. Cells were gradually dehydrated trough an ethanol or acetone series to remove water followed by infiltrated with epoxy resin (SPI), then polymerized at 60°C for 24–48 h to form a rigid block. Sections (70 nm) were cut using ultramicrotome (Leica) and collected on copper grids coated with formvar films. Sections are stained with uranyl acetate (aqueous, 2–5%) for 10–20 minutes to bind nucleic acids and proteins, followed by lead citrate (0.2% in NaOH) for 5–10 minutes to enhance contrast of membranes and cytoplasmic structures.

Excess stain was rinsed with distilled water and dried overnight under a laminar flow hood. The stained sections were observed and imaged under a transmission electron microscope (HITACHI).

Lactate dehydrogenase (LDH) release assay

Cytotoxicity was assessed by LDH release assay using CytoTox 96 Non-Radioactive Cytotoxicity assay kit (Dojindo, CK12) according to the manufacturer's protocols. Briefly, pre-activated $CD8^+$ T cells were resuspended in DMEM culture medium as effector cells and mixed with SJT1601 cells at effector to target ratios equal 20:1. LDH release was detected by absorbance measurement at 490 nm using a colorimetric assay based on the enzymatic reaction of lactate dehydrogenase after culturing at 37ºC for 24 h. Cytotoxicity was calculated according to the formula: Cytotoxicity (%) =(Experimental release − Target cell spontaneous release – effector spontaneous release)/(Target cell maximum release-target cell spontaneous release) × 100 "Experimental release" referred to LDH release from experimental wells. "Target cell spontaneous release" referred to the spontaneous release of LDH from target cells alone. "Effector cell spontaneous release" referred to the spontaneous release of LDH from effector cells alone. "Target cell maximum release" referred to the maximum release of LDH from target cells in a medium containing 1% Triton X-100 T cells.

Immunoprecipitation, Western blot assay and LC-MS/MS

$CD8^+$ T cells or EL4 cells were activated with αCD3/αCD28 for 24 hours. Cell lysates were prepared using RIPA lysis buffer (Thermo) supplemented with protease inhibitor and phosphatase inhibitor (Sigma). The lysates were subjected to immunoprecipitation using an anti-STAT1 antibody (CST, 9172) or an anti-serotonin antibody (Abcam, ab66047) with a Protein G Immunoprecipitation Kit (Thermo, 88802). After normalization of total protein levels, the samples were separated by 10% SDS-PAGE and transferred onto 0.45 μm polyvinylidene difluoride (PVDF) membranes. The membranes were blocked with a protein-free rapid blocking solution (Epizyme) for 30 minutes at room temperature, then cut if necessary and incubated overnight with primary antibodies (1:1000 dilution), followed by incubation with HRP-conjugated secondary antibodies (Abclonal, 1:5000 dilution) for 2 hours. Immunoreactive proteins were visualized using an ECL detection system (Millipore).

To screen for serotonylated proteins, equal amounts of total protein from CD8+ T cell lysates (unstimulated vs. stimulated for 48 hours) were subjected to immunoprecipitation using the anti-serotonin antibody with a Protein A/G Immunoprecipitation Kit. The samples were then separated by 10% SDS-PAGE, but the electrophoresis was run only within a 2 cm length. The resulting gel strips were analyzed by LC-MS/MS at Biotree Technology (Shanghai) Co., Ltd. Briefly, the gel slices were destained with acetonitrile, followed by reduction of disulfide bonds with DTT solution and alkylation with IAA solution. In-gel trypsin digestion

was performed by saturating the gel with trypsin buffer, and peptides were extracted using a formic acid/acetonitrile (ACN) buffer. The extracted peptides were vacuum-dried and reconstituted. Peptides were then separated and analyzed using a nano-UPLC (Evosep One) coupled to a timsTOF Pro2 instrument (Bruker) with a nano-electrospray ion source. Raw MS files were processed using SpectroMine software (version 4.2.230428.52329) and the built-in Pulsar search engine. After the search was completed, qualitative analysis was performed.

Enzymatic serotonylation assays

A 25 μL enzymatic system was established with 5 mM MDC (Sigma) or 5 mM 5-HT, 0.25 μg functional TGM2 protein (R&D, 5418-TG-010) and protein target 10 μg recombinant human STAT1 (Abclonal, RP01251) or 10 μg fibrinogen (Sigma, F3879) and enzymatic buffer (25 mM pH 8 Tris-Cl, 5 mM $CaCl_2$ and protease inhibitor). The reaction buffer was incubated at 37ºC for 3 hours in the dark, then denatured at 98ºC for 8 min prior to gel electrophoresis. Serotonylated proteins were detected under UV illumination, and protein loading was confirmed by Coomassie staining. Peptides of STAT1 were synthesized by Shanghai Sangon Biotechology Co., Ltd. Subsequently, transamidation reactions were carried out using MDC or 5-HT as substrates with 10 μg STAT1 peptides, employing the same protocols as previously described. The serotonylation products were then analyzed by LC-MS/MS.

Enzyme linked immunosorbent assay (ELISA)

5-HT contents of $CD8^+$ T cell cultured supernatants, tumor tissue homogenates (about 0.0100g tissue plus 200 μL RIPA with accurate weight to volume ratio), mouse serum and human plasmas were determined with an ELISA kit (Abnova, KA1894) according to the manufacturer's protocol.

ATP content detection

$CD8^+$ T cells were purified and activated with LDN27219 or Fludarabine for 24 h. El4 cells were activated for 24 h with or without 5-HT. Cells were collected and ATP content was detected using an ATP assay kit (MCE, HY-K0314) according to the manufacturer’s protocol, and protein concentration was measured by BCA assay (Beyotime, P0009). ATP content was normalized to protein content.

Stable transfection of EL4 cells

Lentiviruses-EGFP WT-STAT1 or Gln to Ala (Q120A and Q285) mutated STAT1 plasmids were constructed by OBiO Technology（Shanghai）Co., Ltd. Lentiviral Packaging: transfecting HEK 293T cells with three plasmids: the transfer plasmid, the packaging plasmid (p155/psPAX2), and the envelope plasmid

(pMD2.G). After transfection, the virus-containing supernatants were collected, filtered, and concentrated. EL4 cells were transfected with concentrated supernatants and screened with 8 μg/mL puromycin. The overexpression efficiency was confirmed by flow cytometry analysis.

For overexpression of mtfr2, mCherry-fused lentiviruses expressing mouse mtfr2 were constructed by OBiO Technology（Shanghai）Co., Ltd. El4 cells were transfected at MOI 80 and 8 μg/mL puromycin was add for selection.

siRNA interference experiment

MTFR2 knockdown in El4 cells was established by transfection with small interfering RNA (siRNA) using CALNP™ RNAi in vitro agent (D-nano therapeutics, Beijing, China) according to the manufacturer's instructions. *Mtfr2* siRNA (si*Mtfr2*): 5'- CGACUUGAGUGAUGAACA ATT-3', and negative control siRNA (siNC) were provided by OBiO Technology（Shanghai）Co., Ltd.

Real-time qPCR

Total RNA was isolated from activated $CD8^+$ T cells or EL4 cells using TRIzol reagent (Thermo) following the manufacturer's protocol. First-strand cDNA synthesis was performed using the PrimeScript RT reagent Kit (Takara, RR037B) according to the manufacturer's protocol. 10 ng of synthesized cDNA served as the template for real- time qPCR analysis. Gene expression quantification was carried out using SYBR Green Pro Taq HS qPCR Master Mix (Accurate Bio). Amplification conditions consisted of 40 cycles: denaturation at 95°C for 15 s, annealing at 60°C for 15 s, and extension at 72°C for 45 s. Target gene primers are listed in the Key Resources Table. Relative gene expression levels were normalized to the housekeeping gene *hprt* using the comparative cycle threshold ($2^{-\Delta\Delta CT}$) method. The primers were listed in the key resources table. qPCR was performed using the following primers: *Hprt* forward, 5'- GTTGGGCTTACCTCACTGCT-3' and reverse, 5'- TAATCACGACGCTGGGACTG -3'; *Mfn2* forward, 5'- GCTAGTGACGTGTTGGGTGT-3' and reverse, 5'-GGTGTTGACTCCA CCTGTCC-3'; *Mtfr2* forward, 5'-AGCTCCAGGGATGGTGATCTT-3' and reverse, 5'- GCAAATCCTGGTCTACGGGA-3'; *Dnm1l* forward, 5'- ACCGGGAATGACCAAAGTACC-3' and reverse, 5'- TGGGATTACTGATGAACCGAAGA-3'.

ChIP qPCR

The ChIP assay was performed using the Pierce Magnetic ChIP Kit (26157, Thermoscientific) according to the manufacturer's instructions. Briefly, dead cells were removed by the Ficoll density gradient centrifugation. 8-10 × 10^6 activated $CD8^+$ cells were washed and Crosslinked with 1% formaldehyde for 10

min and stop with glycine. Then, cells were lysed to remove the cell membrane and isolate nuclei. Chromatin was then digested with Micrococcal Nuclease (MNase) to generate fragments of approximately 150–300 bp. Following MNase inactivation, the nuclear membrane was disrupted to release the digested chromatin. The resulting chromatin fragments were subjected to immunoprecipitation using Phospho-Stat1 (Ser727) antibodies (CST, #8826). After washing, DNA was eluted, cross-links were reversed, and DNA was purified. Purified DNA was analyzed by qPCR. *Mfn2* promoter primer: forward, 5'-CTGGTAACCGTCCCGTGTC-3' and reverse, 5'-CGGACGCTGATCCAAACTACA-3'. *Mtfr2* promoter primer1: forward, 5'-TAGGACAGACTTGGAGGA ACTG-3' and reverse, 5'- AAAGTTGGCTTTGAAATGCTGCC-3'. *Mtfr2* promoter primer2: forward, 5'- TGTGGTTTCCTTAGTGCGGT-3' and reverse, 5'- ACGCTGTTCGTTG GTACCTT -3'.

RNA sequencing

$CD8^+$ T cells were activated with αCD3/αCD28 for 24 h with or without 50μM LDN27279. Total RNAs were isolated using the TRIzol reagent following the manufacturer's protocol. RNA integrity was assessed by Agilent 4200 Bioanalyzer (RIN ⩾ 6.0). Samples were sent to GENE DENOVO biotechnology for clustering and sequencing.

Human ChIP-seq analysis

Human ChIP-seq data (GSE100566 and GSM4304440) analysed in a web platform named H^3NGST[47], and and visualized with Integrative Genomics Viewer (IGV).

Human single-cell RNA sequencing analysis

Public scRNA-seq datasets GSE189357 (TD1-TD9) and GSE207422 (anti-PD-1/chemotherapy cohort: Pre, n=3; NR, n=8; R, n=4) were analyzed using Scanpy in Python 3. After quality control and UMAP dimensionality reduction, cell types were annotated using canonical markers. Samples from GSE189357 were stratified into TPH1_high and TPH1_low groups based on median *TPH1* expression; $CD8^+$ T cells were extracted for subclustering and functional scoring, and *PD-1* expression was compared between groups. For the independent cohort (GSE207422), pseudobulk analysis (raw count aggregation per Sample × cell type, followed by CPM + log2 normalization) was used to evaluate TPH1 expression in T and B cells. PyDESeq2 was applied for between-group differential expression comparison, and the proportion of $TPH1^+$ samples was calculated per response group. Statistical comparisons were performed using Mann-Whitney U test or ANOVA as appropriate.

Statistical analysis

The sample size, statistical methods, and relevant details are provided in the figure legends. Statistical analysis was performed with Graphpad Prism 7, and values were presented as mean ± standard error of the mean (SEM). Data were analyzed using appropriate statistical tests, including two-tailed student's t-test, one-way ANOVA and Tukey's test, and two-way ANOVA. The Spearman correlation test was applied to perform the association analysis. *p < 0.05, **p < 0.01, ***p < 0.001; ns, no significance.

References

1. Khalil, D.N., Smith, E.L., Brentjens, R.J. & Wolchok, J.D. The future of cancer treatment: immunomodulation, CARs and combination immunotherapy. *Nat Rev Clin Oncol* **13**, 273-290 (2016).
2. Ribas, A. & Wolchok, J.D. Cancer immunotherapy using checkpoint blockade. *Science* **359**, 1350-1355 (2018).
3. Chow, A., Perica, K., Klebanoff, C.A. & Wolchok, J.D. Clinical implications of T cell exhaustion for cancer immunotherapy. *Nat Rev Clin Oncol* **19**, 775-790 (2022).
4. Nayak, L.*, et al.* PD-1 blockade with nivolumab in relapsed/refractory primary central nervous system and testicular lymphoma. *Blood* **129**, 3071-3073 (2017).
5. Le, D.T.*, et al.* PD-1 Blockade in Tumors with Mismatch-Repair Deficiency. *N Engl J Med* **372**, 2509-2520 (2015).
6. Park, J., Hsueh, P.C., Li, Z. & Ho, P.C. Microenvironment-driven metabolic adaptations guiding CD8(+) T cell anti-tumor immunity. *Immunity* **56**, 32-42 (2023).
7. Li, H.*, et al.* Optimizing mitochondria function in immune cells: implications for cancer immunotherapy. *Trends Cancer* **11**, 1170-1184 (2025).
8. Huang, Y.*, et al.* Rewiring mitochondrial metabolism to counteract exhaustion of CAR-T cells. *J Hematol Oncol* **15**, 38 (2022).
9. Vardhana, S.A.*, et al.* Impaired mitochondrial oxidative phosphorylation limits the self-renewal of T cells exposed to persistent antigen. *Nat Immunol* **21**, 1022-1033 (2020).
10. Chen, X.*, et al.* Mitochondrial Regulation of CD8 T Cells: Mechanisms and Therapeutic Modulation. *Adv Sci* **12**(2025).
11. Yang, M.Q.*, et al.* Targeting mitochondria: restoring the antitumor efficacy of exhausted T cells. *Mol Cancer* **23**, 260 (2024).

12. Wu, H., *et al.* Mitochondrial dysfunction promotes the transition of precursor to terminally exhausted T cells through HIF-1α-mediated glycolytic reprogramming. *Nat Commun* **14**(2023).
13. Monje, M., *et al.* Roadmap for the Emerging Field of Cancer Neuroscience. *Cell* **181**, 219-222 (2020).
14. Vermeer, P.D., Restaino, A.C., Barr, J.L., Yaniv, D. & Amit, M. Nerves at Play: The Peripheral Nervous System in Extracranial Malignancies. *Cancer Discov* **15**, 52-68 (2025).
15. Amit, M., *et al.* Neuro-immune cross-talk in cancer. *Nat Rev Cancer* **25**, 573-589 (2025).
16. Vahid-Ansari, F. & Albert, P.R. Rewiring of the Serotonin System in Major Depression. *Front Psychiatry* **12**(2021).
17. Ye, D., *et al.* The role of 5-HT metabolism in cancer. *Biochim Biophys Acta Rev Cancer* **1876**, 188618 (2021).
18. Bosakova, V., *et al.* Serotonin attenuates tumor necrosis factor-induced intestinal inflammation by interacting with human mucosal tissue. *Exp Mol Med* **57**, 364-378 (2025).
19. Reddy, A.P., *et al.* Role of Serotonylation and SERT Posttranslational Modifications in Alzheimer's Disease Pathogenesis. *Aging Dis* **16**, 841-858 (2025).
20. Walther, D.J., *et al.* Serotonylation of small GTPases is a signal transduction pathway that triggers platelet α-granule release. *Cell* **115**, 851-862 (2003).
21. Watts, S.W., Priestley, J.R.C. & Thompson, J.M. Serotonylation of Vascular Proteins Important to Contraction. *Plos One* **4**(2009).
22. Hummerich, R., Thumfart, J.O., Findeisen, P., Bartsch, D. & Schloss, P. Transglutaminase-mediated transamidation of serotonin, dopamine and noradrenaline to fibronectin: Evidence for a general mechanism of monoaminylation. *Febs Lett* **586**, 3421-3428 (2012).
23. Lee, T.A., *et al.* Post-translational Modification of PD-1: Potential Targets for Cancer Immunotherapy. *Cancer Res* **84**, 800-807 (2024).
24. Liu, Y., *et al.* Activation and antitumor immunity of CD8
T cells are supported by the glucose transporter GLUT10 and disrupted by lactic acid. *Sci Transl Med* **16**(2024).
25. Wang, X., *et al.* A GAPDH serotonylation system couples CD8(+) T cell glycolytic metabolism to antitumor immunity. *Mol Cell* **84**, 760-775 e767 (2024).
26. Li, B., *et al.* Serotonin transporter inhibits antitumor immunity through regulating the intratumoral serotonin axis. *Cell* **188**, 3823-3842 e3821 (2025).
27. Schneider, M.A., *et al.* Attenuation of peripheral serotonin inhibits tumor growth and enhances immune checkpoint blockade therapy in murine tumor models. *Sci Transl Med* **13**, eabc8188 (2021).

28. Ling, T.*, et al.* Serotonylation in tumor-associated fibroblasts contributes to the tumor-promoting roles of serotonin in colorectal cancer. *Cancer Lett* **600**, 217150 (2024).
29. Lin, S.*, et al.* Histone serotonylation promotes pancreatic cancer development via lipid metabolism remodeling. *Nat Commun* **16**, 5947 (2025).
30. Ji, Y.*, et al.* Serotonin modulates lineage plasticity in neuroendocrine prostate cancer via epigenetic reprogramming. *Cancer Discov* (2025).
31. Zhao, Z.*, et al.* Inhibition of stromal MAOA leading activation of WNT5A enhance prostate cancer immunotherapy by involving the transition of cancer-associated fibroblasts. *J Immunother Cancer* **13**(2025).
32. Huang, Q.*, et al.* The primordial differentiation of tumor-specific memory CD8(+) T cells as bona fide responders to PD-1/PD-L1 blockade in draining lymph nodes. *Cell* **185**, 4049-4066 e4025 (2022).
33. Gamero, A.M. & Larner, A.C. Signaling via the T cell antigen receptor induces phosphorylation of Stat1 on serine 727. *J Biol Chem* **275**, 16574-16578 (2000).
34. Zhang, L.*, et al.* MTFR2-Mediated Fission Drives Fatty Acid and Mitochondrial Co-Transfer from Hepatic Stellate Cells to Tumor Cells Fueling Oncogenesis. *Adv Sci (Weinh)* **12**, e2416419 (2025).
35. Philips, R.L.*, et al.* The JAK-STAT pathway at 30: Much learned, much more to do. *Cell* **185**, 3857-3876 (2022).
36. Zeng, Y.*, et al.* IFI44L as a novel epigenetic silencing tumor suppressor promotes apoptosis through JAK/STAT1 pathway during lung carcinogenesis. *Environ Pollut* **319**, 120943 (2023).
37. Gil, K.B.*, et al.* The STAT3-VDAC1 axis modulates mitochondrial function and plays a critical role in the survival of acute myeloid leukemia cells. *Haematologica* (2025).
38. Comita, S.*, et al.* Regulation of STAT3 and its role in cardioprotection by conditioning: focus on non-genomic roles targeting mitochondrial function. *Basic Res Cardiol* **116**, 56 (2021).
39. Odell, A.V.*, et al.* EGFR-STAT1 pathway drives fibrosis initiation in fibroinflammatory skin diseases. *Nat Commun* **16**, 8969 (2025).
40. Yang, J.*, et al.* Trophoblast-derived miR-410-5p induces M2 macrophage polarization and mediates immunotolerance at the fetal-maternal interface by targeting the STAT1 signaling pathway. *J Transl Med* **22**, 19 (2024).
41. Bancerek, J.*, et al.* CDK8 kinase phosphorylates transcription factor STAT1 to selectively regulate the interferon response. *Immunity* **38**, 250-262 (2013).
42. Putz, E.M.*, et al.* CDK8-mediated STAT1-S727 phosphorylation restrains NK cell cytotoxicity and tumor surveillance. *Cell Rep* **4**, 437-444 (2013).

43. Bartalucci, N.*, et al.* A Novel, Ruxolitinib-Sensitive, CCDC6::JAK2 Fusion Gene in a Patient With Atypical, JAK2 Unmutated, Polycythemia Vera-Like, Myeloproliferative Neoplasm. *Am J Hematol* **101**, 379-383 (2026).
44. Annawald, K., Gregus, A., Wirths, O. & Meyer, T. Characterization of a pathogenic gain-of-function mutation in the N-terminal domain of STAT1 which is reported to be associated with eosinophilic esophagitis. *Cell Commun Signal* **23**, 367 (2025).
45. He, X.*, et al.* Lysine vitcylation is a vitamin C-derived protein modification that enhances STAT1-mediated immune response. *Cell* **188**, 1858-1877 e1821 (2025).
46. Yao, C.C.*, et al.* Accumulation of branched-chain amino acids reprograms glucose metabolism in CD8(+) T cells with enhanced effector function and anti-tumor response. *Cell Rep* **42**, 112186 (2023).
47. Heo, H.H. & Um, S.J. H(3)NGST: a fully automated, web-based platform for end-to-end ChIP-seq analysis. *BMC Bioinformatics* **26**, 243 (2025).

Figure 1.

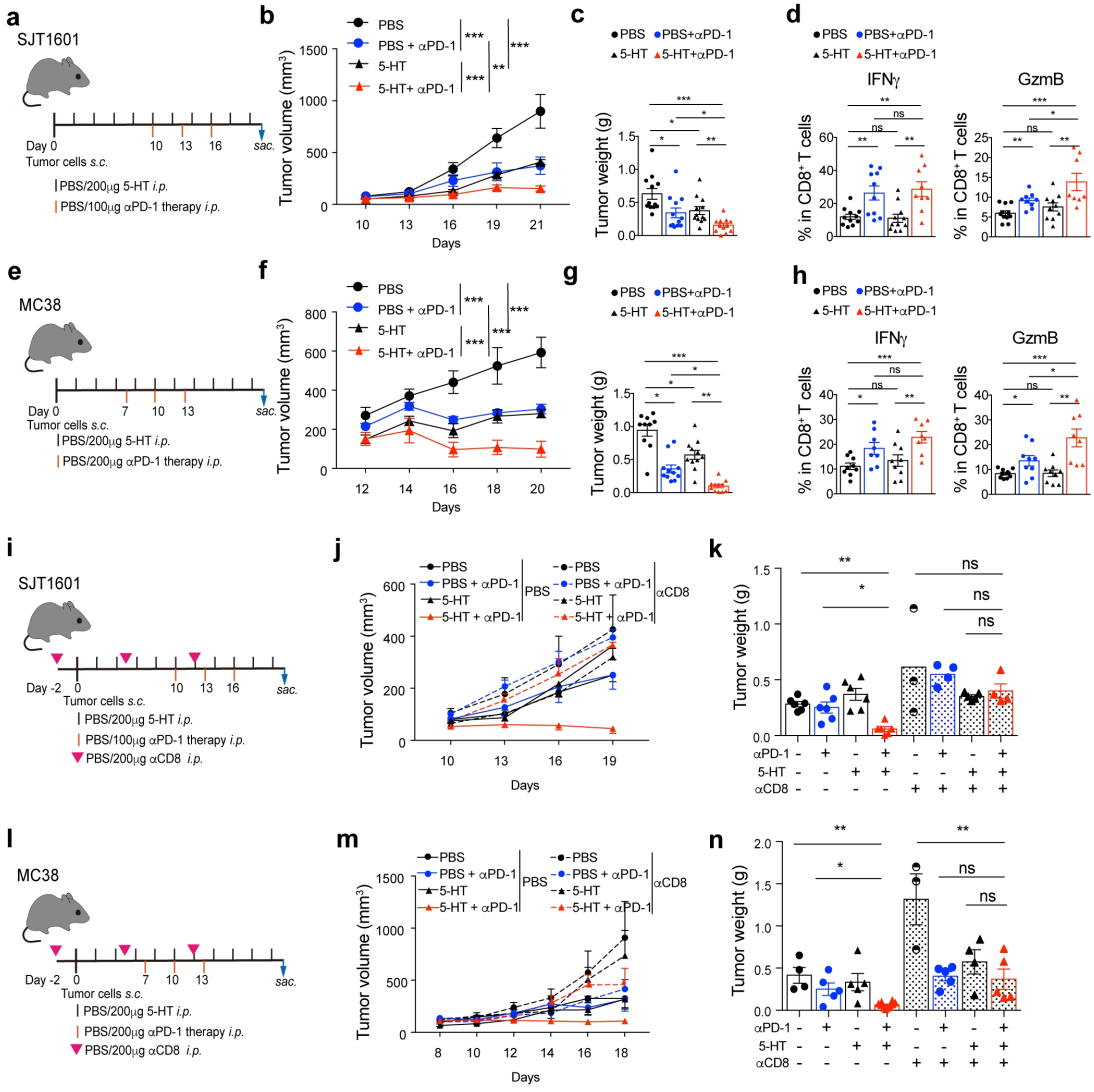

Fig.1 5-HT supplementation exhibit enhanced CD8⁺ T cell functionality and synergizes with anti-PD-1 to inhibit tumor growth

a-d Studying SJT1601 tumor growth. Schematic timeline (**a**)**,** tumor growth curve (**b**)., tumor weight (**c**), and FACS analyses of IFNγ⁺ and GzmB⁺ in tumor infiltrating CD8⁺ T cells (**d**) (n = 8-12, Data from two independent experiments were pooled). **e-h** Studying MC38 tumor growth. Schematic timeline (**e**)**,** tumor growth curve (**f**)**,** tumor weight (**g**), and FACS analyses of IFNγ⁺ and GzmB⁺ in tumor infiltrating CD8⁺ T cells (**h**) (n = 8-10, Data from two independent experiments were pooled). **i-k** Studying SJT1601 tumor growth with anti-CD8a antibody. Experimental design (**i**)**,** tumor growth curve (**j**)**,** and tumor weight (**k**) (n = 3-6). **l-n** Studying MC38 tumor growth with anti-CD8a antibody. Experimental design (**l**), tumor growth curve (**m**), and tumor weight (**n**) (n = 3-5). Data are presented as mean ± SEM. Statistical analyses were performed using one-way ANOVA and Tukey's test (**c**, **d**, **g**, **h**, **k** and **n**) and two-way ANOVA and Tukey's test (**b** and **f**). ns, non-significant; *$p < 0.05$, **$p < 0.01$, ***$p < 0.001$.

Figure 2.

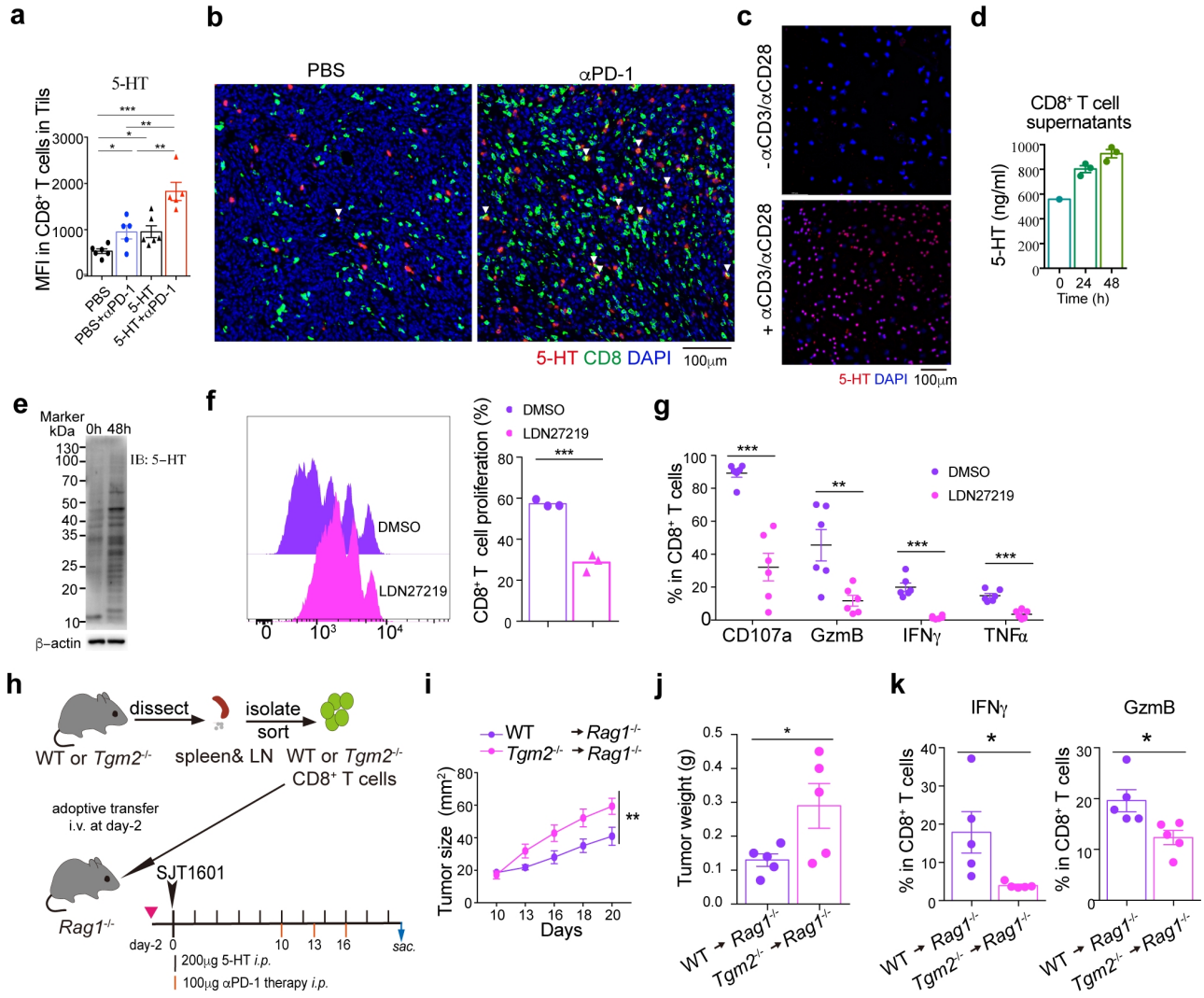

Fig. 2 Serotonylation via TGM2 is required for CD8$^+$ T cell antitumor function.

a, FACS analysis of 5-HT expression in tumor infiltrating CD8$^+$ T cells from SJT1601 tumor-bearing mice after treatment with PBS versus 5-HT with or without anti-PD-1 antibody (n = 5-6). **b**, Immunofluorescence staining of CD8a and 5-HT in SJT1601 grafted tumors from the mice treated with or without anti-PD1 antibody. Green indicates CD8a and Red (AF594) indicates 5-HT. Blue (DAPI) indicates the nucleus. White arrows show co-location of CD8 and 5-HT. Scale bar, 100 μm (n = 5). **c**, Immunofluorescence staining of 5-HT in CD8$^+$ T cells with or without αCD3/αCD28 for 24 h. Red indicates 5-HT and blue indicates the nucleus. Scale bar, 100 μm (n = 3). **d**, Concentrations of 5-HT in CD8$^+$ T cell supernatants stimulated with αCD3/αCD28 for 0, 24 h and 48 h by ELISA (n = 1-3). **e**, Immunoblotting analysis of 5-HT and β-actin in CD8$^+$ T cells with αCD3/αCD28 stimulation for 0 or 48 h. **f**, proliferation analysis of CD8$^+$ T cells with or without LDN27219 treatment for 72 h with CFSE pre-staining (n = 3). **g**, Intracellular cytokines analysis of CD8$^+$ T cells with or without LDN27219 treatment for 48 h (n = 6). **h-k,** Experimental design for WT or

Tgm2$^{-/-}$ CD8^{+} T cells adoptive transfer to *Rag1*$^{-/-}$ mice followed by SJT1601 subcutaneously implanted (**h**), tumor growth curve (**i**) and tumor weight at day 21 (**j**) were measured. Percentages of IFNγ and GzmB in tumor infiltrating CD8^{+} T cells were detected by FACS (**k**). (n = 4-5). Representative of two (**a**, **b**, **c**, **e**, **f**, **i**, **j**) and three (**f**, **g**) experiments. Data are presented as mean ± SEM. Statistical analyses were performed using one-way ANOVA and Tukey's test (**a**), two-way ANOVA and Tukey's test (**i**) and unpaired Student's t-test (**f**, **g**, **j** and **k**). ns, non-significant; $^{*}p < 0.05$, $^{**}p < 0.01$, $^{***}p < 0.001$.

Figure 3.

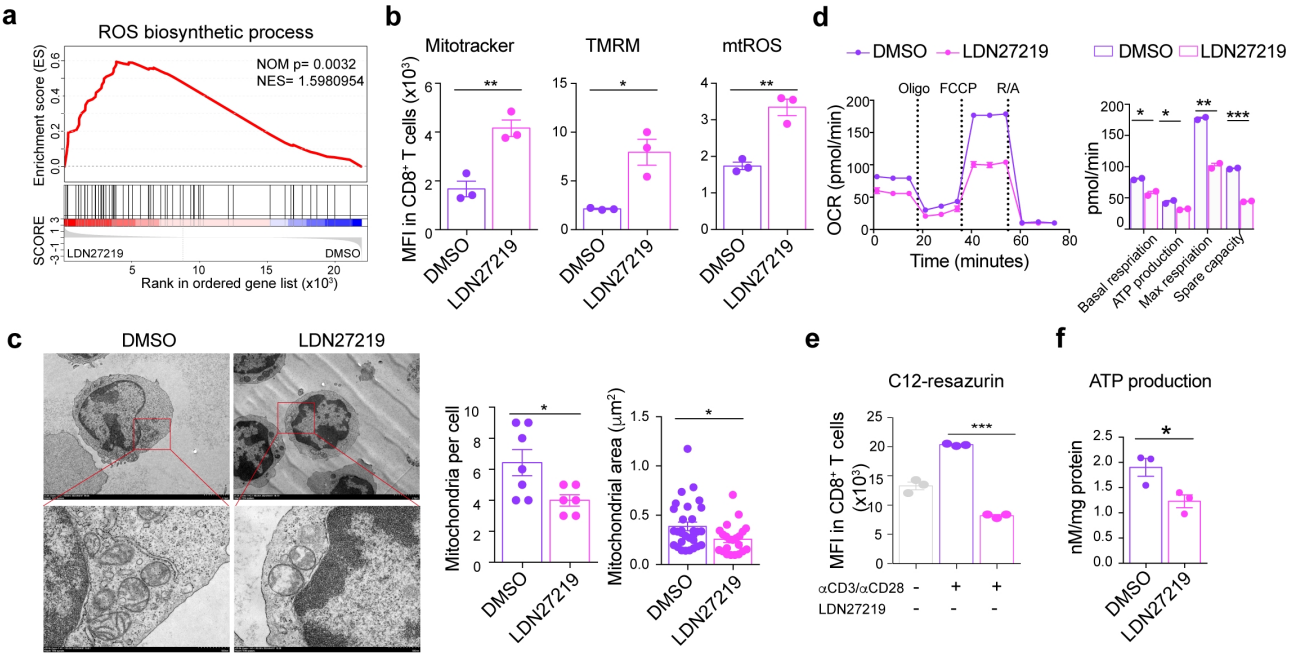

Fig. 3 Inhibition of serotonylation impairs mitochondrial function in $CD8^+$ T cells

a, GSEA analysis of the ROS biosynthetic process between DMSO and LDN27219-treated $CD8^+$ T cells (n = 3). **b**, $CD8^+$ T cells were activated for 24 h, with or without LDN27219 treatment. Mitotracker, TMRM and mitoSOX were stained (n = 3). **c**, $CD8^+$ T cells were activated for 24 h, with or without LDN27219 treatment. Electron Micrograph of Mitochondria and Structural Diagram were displayed by transmission electron microscopy. Mitochondria numbers of each cells and mitochondrial area were statistically analyzed (n = 6-7). **d**, $CD8^+$ T cells were activated for 48 h, with or without LDN27219 treatment. OCR was measured, basal respiration, ATP production, Max respiration and spare capacity were analyzed (n = 2). **e**, $CD8^+$ T cells were activated for 24 h, with or without LDN27219 treatment. C12-resazurin staining were conducted (n = 3). **f**, $CD8^+$ T cells were activated for 24 h, with or without LDN27219 treatment. ATP productions were measured (n = 3). Representative of two (**d**, **f**) and three (**b**, **e**) experiments. Data are presented as mean ± SEM. ns, non-significant; $^*p < 0.05$, $^{**}p < 0.01$, $^{***}p < 0.001$ by the unpaired Student's t-test.

Figure 4.

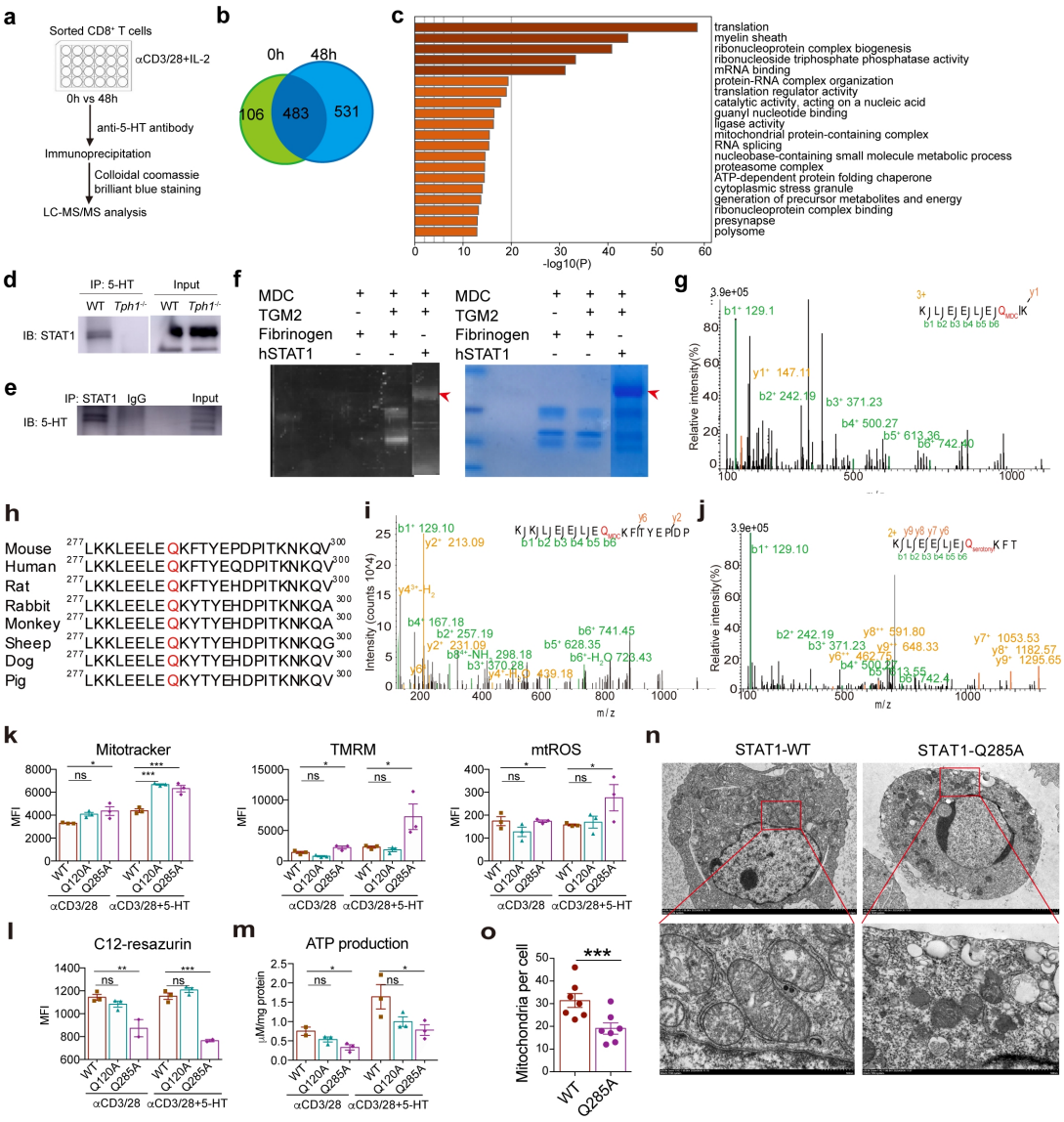

Fig. 4 Serotonylation of STAT1 prevents mitochondrial dysfunction and maintains effector function in CD8$^+$ T cells

a, Workflow for the discovery of serotonylated proteins by LC-MS/MS. **b**, Venn diagram showing the overlap of serotonylated proteins between 0 h and 48 h activated CD8$^+$ T cells. **c**, Enrichment of KEGG pathways upregulated in CD8$^+$ T cells from 48 h. **d**, WT and *Tph1*$^{-/-}$ CD8$^+$ T cells were activated for 48 h, 5-HT was immunoprecipitated, and STAT1 was detected. **e**, CD8$^+$ T cells were activated for 48 h, STAT1 or IgG was immunoprecipitated, and 5-HT was detected. **f**, TGM2 monoaminylation assays with STAT1 or fibrinogen were shown through UV light and then stained with coomassie brilliant blue staining. **g**, LC-MS/MS analysis of TGM2-transamidated MDC to human recombinant STAT1.**h**, The gene similarity of STAT1 across different species. **i**, LC-MS/MS analysis of TGM2-transamidated MDC to mouse STAT1

peptide 277-295. **j**, LC-MS/MS analysis of TGM2-transamidated 5-HT to mouse STAT1 peptide 277-295. **k-m**, EL4 cells were transfected with lentiviruses expressing either WT-STAT1 or Gln to Ala (Q120A and Q285A) mutated STAT1. Cells were activated for 24 h, with or without 100 μM 5-HT. Mitotracker, TMRM and mitoSOX were analyzed by FACS (n = 3) (**k**). C12-resazurin staining were conducted (n = 3) (**l**). ATP production was detected (n = 3) (**m**). **n**, EL4 T cells were activated for 24 h with 5-HT. Electron Micrograph of Mitochondria and Structural Diagram were displayed by transmission electron microscopy. **o**, Mitochondria numbers of each cells in the **n** were statistically analyzed (n = 8). Representative of two experiments. Data are presented as mean ± SEM. Statistical analyses were performed using one-way ANOVA and Tukey's test (**k**, **l, m** and **o**) and unpaired Student's t-test (**h**). ns, non-significant; $^{*}p < 0.05$, $^{**}p < 0.01$, $^{***}p < 0.001$.

Figure 5.

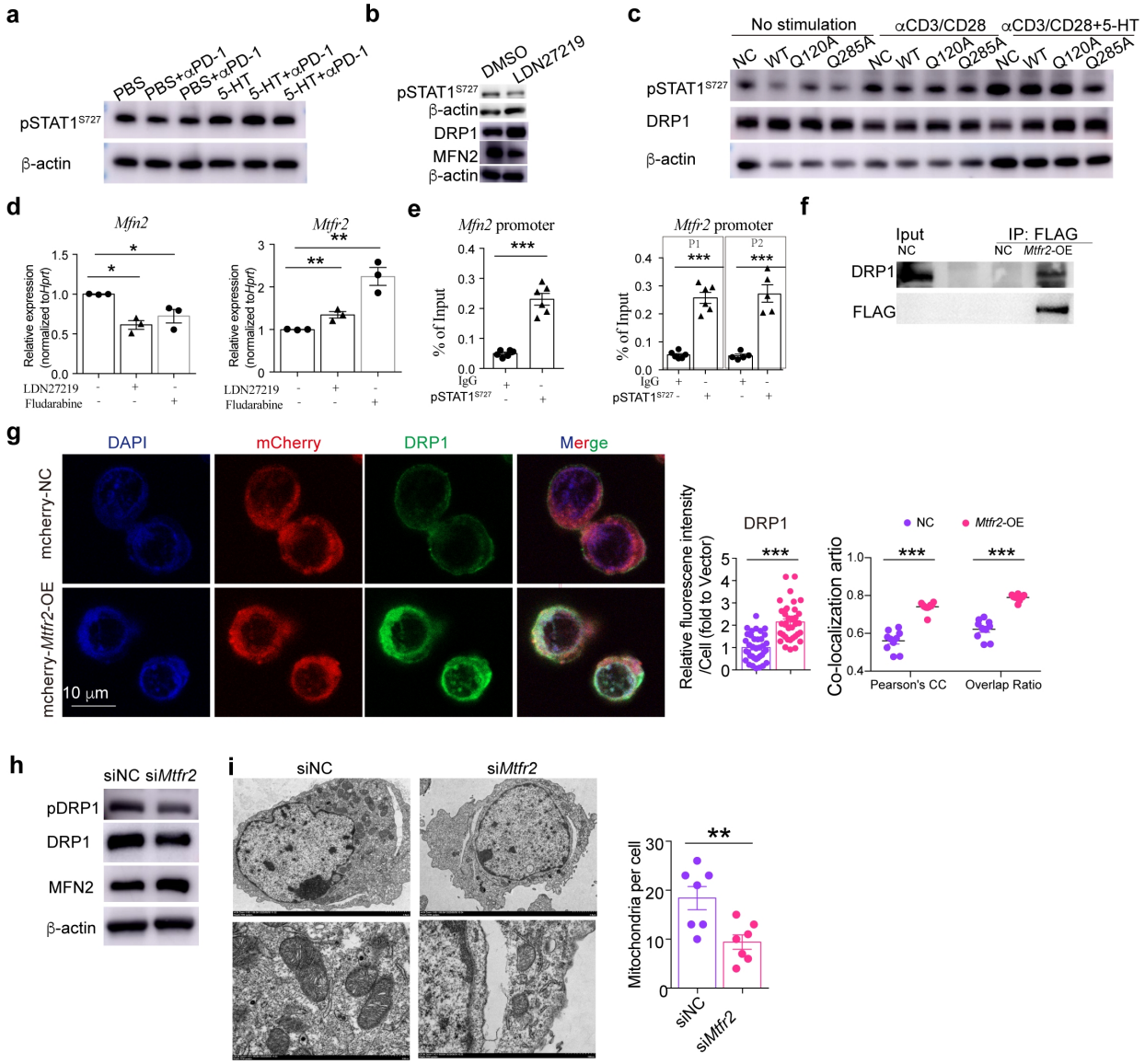

Fig. 5 Serotonylation of Gln285 at STAT1 facilitates its Ser727 phosphorylation and regulates mitochondrial dynamics

a, Western blot analysis of indicated proteins in purified TdLN CD8$^+$ T cells from SJT1601 tumor-bearing mice after treatment with PBS versus 5-HT with or without anti-PD-1 antibody (n = 1-2 pooled). **b**, CD8$^+$ T cells were activated for 24 h with or without LDN27219. Indicated proteins were detected by western blot. **c**, Transected WT or mutated STAT1 EL4 cells were activated for 24 h with or without 100 μM 5-HT. Indicated proteins were detected by western blot. **d,** ***Mfn2*** **and** *Mtfr2* mRNA expressions in CD8$^+$ T cells treated with LDN27219 or fludarabine **for 24 h** were analyzed by qPCR (n = 3). **e**, ChIP was performed with an anti-pSTAT1^{S727} antibody or control IgG on activated CD8$^+$ T cells. The precipitated DNA was analyzed by qPCR with one pair of primers targeting the *Mfn2* promoter and two pairs of primers targeting distinct regions of the *Mtfr2* promoter. Data are presented as percentage of input DNA (n = 6). **f-g,** mCherry-fused

lentiviruses with Flag-label expressing MTFR2 was transduced into EL4 cells. Flag was immunoprecipitated, and DRP1 was detected (**f**). Immunofluorescence staining of DRP1, Green indicates DRP1 and Red (mCherry) indicates negative control (NC) or *Mtfr2*-OE. Middle: DRP1 fluorescence intensity analysis. Right: colocalization analysis of mCherry-tagged MTFR2 and DRP1 (green), Pearson's Correlation Coefficient and Overlap Ratio were calculated from 10 slices per condition. Blue (DAPI) indicates the nucleus. Scale bar, 100 μm (**g)**. **h-i,** EL4 cells were transfected with 40 nM of *Mtfr2* siRNA (si*Mtfr2*) or a negative control siRNA (siNC), and then activated for 24 h. Indicated proteins were analyzed by western blot (**h**). Mitochondria and structural diagram were displayed by transmission electron microscopy. Mitochondria numbers of each cells were statistically analyzed (**i)**. Representative of two experiments. Data are presented as mean ± SEM. ns, non-significant; $^{*}p < 0.05$, $^{**}p < 0.01$, $^{***}p < 0.001$ by the unpaired Student's t-test.

Figure 6.

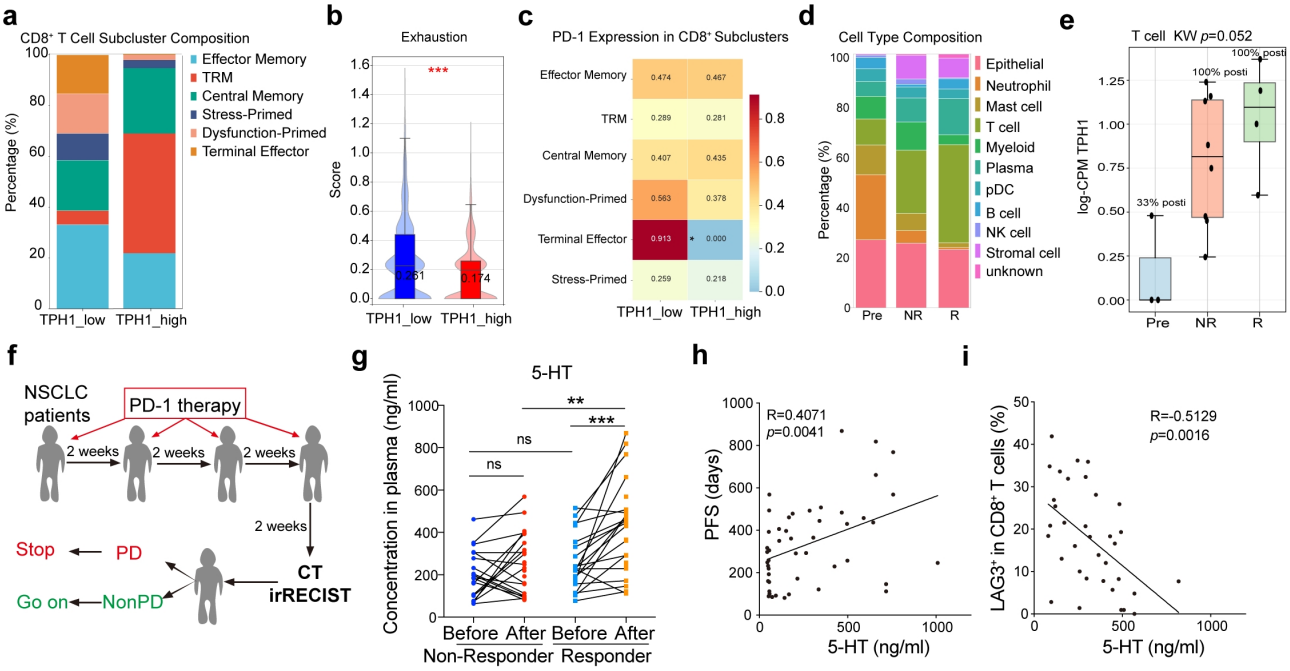

Fig. 6 Clinical relevance of 5-HT in anti-PD-1 therapy in non-small cell lung cancer

a-c Human NSCLC tumor samples scRNA-seq dataset analysis (GSE189357). Stacked bar chart showing $CD8^+$ T cell subset distribution in TPH1_low vs TPH1_high groups (**a**). Violin plots of $CD8^+$ T cell exhaustion function score from TPH1_low vs TPH1_high tumors (**b**). Heatmap showing PD-1 expression levels across $CD8^+$ T cell subsets stratified by TPH1 group (**c**). **d-e** Human NSCLC tumor samples before and after anti-PD-1+chemotherapy scRNA-seq dataset analysis (GSE207422). Stacked bar charts showing Immune cell composition changes following treatment (**d**). TPH1 expression dynamics in T cells across treatment response groups (**e**). **f-i** Analysis of NSCLS patients with nivolumab treatment. Flowchart for nivolumab treatment in NSCLS patients (**f**). 5-HT levels in the plasma of the responder versus the non-responder NSCLC patients at the baseline or received therapy for 4 weeks. (n = 22/24) (**g**). Spearman correlations of plasma 5-HT levels with progression-free survival (PFS) (**h**). Spearman correlations of plasma 5-HT levels with the percentages of $LAG3^+$ $CD8^+$ T cells in PBMC (**i**). Data are presented as mean ± SEM. Statistical analyses were performed using Ma -Whitney U test in (**b, c**), Kruskal-Wallis test in (**e**), paired Student's t-test in (**g**). $^*p < 0.05$, $^{**}p < 0.01$, $^{***}p < 0.001$.

Table1— Clinical manifestations of advanced NSCLC patients receiving nivolumab treatment

Characteristics	NR (22)	R (24)	*p* Value
Age, y median	60.3 ± 2.004	57.9 ± 1.725	0.3691
Gender Male Female	 15 (68.18) 7 (31.82)	 21 (87.5) 3 (12.5)	 0.1586
Disease stage III IV	 4 (18.18) 18 (81.82)	 8 (33.33) 16 (66.67)	 0.3214
History Squamous nonsquamous	 8 (36.36) 14 (63.64)	 9 (37.5) 15 (62.5)	 >0.9999
Metastasis Yes No	 19 (86.36) 3 (13.64)	 18 (75) 6 (25)	 0.4638
EGFR mutation Yes No	 1 (4.55) 21 (95.45)	 1 (4.17) 23 (95.83)	 >0.9999

Values are n (%) unless otherwise stated.

R, responder; NR, non-responder.

Inventory of Supporting Information

Figure#	Figure title	Filename	Figure Legend
Extended Data Fig. 1	5-HT enhances anti-PD-1 efficacy via modulating $CD8^+$ T cell exhaustion, memory, and cytotoxicity, independent of NK cells	**Extended Data Fig. 1**	**a**, Serum 5-HT levels of SJT1601 tumor-bearing mice treatment with PBS, αPD-1, 5-HT or 5-HT+ αPD-1 (n = 5). **b**, SJT1601 tumor Photos. **c**, Percentages of KLRG and LAG3 in SJT1601 tumor infiltrating $CD8^+$ T cells from indicated treated mice (n = 5-6). **d**, NK cell percentages and cytokine production of NK cells in tumors from indicated treated mice (n = 4-6). **e**, FACS analysis of CD44 and CD62L expression in TdLN $CD8^+$ T cells from indicated treated mice (n = 6). **f**, $CD8^+$ T cells purified from TdLNs, reactivated and coculture with SJT1601 in vitro, tumor apoptosis was detected and LDHa release was measured (n = 4). **g**, MC38 tumor Photos. **h**, SJT1601 tumor Photos of mice administrated with or without CD8 depletion. **i**, MC38 tumor Photos of mice administrated with or without CD8 depletion. Data are presented as mean ± SEM. ns, non-significant; $^*p < 0.05$, $^{**}p < 0.01$, $^{***}p < 0.001$ by one-way ANOVA with Tukey's test.
Extended Data Fig. 2	**Anti-PD-1 upregulates tumor 5-HT and** serotonin inhibition impairs $CD8^+$ T cell functionality	**Extended Data Fig. 2**	**a**, Concentration of 5-HT in MC38 tumor from mice treated with or without anti-PD-1 therapy (n = 7). **b**, $CD8^+$ T cells activated for 0 or 24 h in the presence or absence of LDN27219, followed by immunoblotting analysis of 5-HT and β-actin. **c**, $CD8^+$ T cells were activated for 24 h with or without LDN-27219; RNA sequencing was then performed, followed by gene ontology (GO) biological process analysis (n = 3). **d**, GSEA of cytokine activity in $CD8^+$ T cells treated with DMSO or LDN27219 (n = 3). Data are presented as

			mean ± SEM. $^{**}p < 0.01$ by the unpaired Student's t-test.
Extended Data Fig. 3	Seahorse analysis of glycolytic function in activated $CD8^+$ T cells treated with or without LDN27219	**Extended Data Fig. 3**	**a**, $CD8^+$ T cells were activated for 48 h with or without LDN27219 treatment, and extracellular acidification rate (ECAR) was measured using a Seahorse analyzer. **b**, Basal glycolysis and glycolytic capacity were analyzed based on the data in (**a)**. Representative of two independent experiments. Data are presented as mean ± SEM. *p* values were analyzed using the unpaired Students's t-test.
Extended Data Fig. 4	TGM2-mediated transamidation of MDC and 5-HT to STAT1 at Gln120 and validation of STAT1 mutants in EL4 cells	**Extended Data Fig. 4**	**a**, LC-MS/MS analysis of TGM2-transamidated MDC to human recombinant STAT1. **b**, LC-MS/MS analysis of TGM2-transamidated MDC to mouse STAT1 peptide 108-126. **c**, LC-MS/MS analysis of TGM2-transamidated 5-HT to mouse STAT1 peptide 108-126. **d,** Transfection efficiency of STAT1-WT, and STAT1-Q120A and STAT1-Q285A mutant viruses in EL4 cells.
Extended Data Fig. 5	Fludarabine treatment exacerbates $CD8^+$ T cell exhaustion and reduces tumor cell cytotoxicity	**Extended Data Fig. 5**	**a-c** $CD8^+$ T cells were activated for 24 h with 0, 5 or 10 μm fludarabine. Staining with Mitotracker, TMRM and mitoSOX (**a**), measurement of ATP production (**b**) and staining of cytokines (**c**) (n = 4). **d-f Exhausted $CD8^+$ T cells were induced in vitro** with 0, 5, or 10 μM fludarabine. Study design (**d**). FACS analysis of exhaustion-related marker expression (n = 2) (**e**). **In vitro** induced exhausted $CD8^+$ T cells coculture with SJT1601 tumor cells, the cell cytotoxicity was analyzed by LDH release (n = 3) (**f**). Statistical analyses were performed using one-way ANOVA and Tukey's test (**a-c**, **e**) and the paired Student's t test (**f**). Representative of

			two experiments. Data are presented as mean ± SEM. ns, non-significant; *$p < 0.05$, **$p < 0.01$, ***$p < 0.001$ by the unpaired Student's t-test.
Extended Data Fig. 6	Effects of PP2, LDN27219, and fludarabine on pSTAT1^{S727}, *Dnm1l* expression, and chromatin signatures at MFN2 and MTFR2 loci, along with *Mtfr2* knockdown efficiency	**Extended Data Fig. 6**	**a**, CD8$^+$ T cells activated for 0, 24 h, with or without 10 μM PP2. Immunoblotting analysis of pSTAT1^{S727}and β-actin. **b**, ***Dnm1l*** mRNA expressions in CD8$^+$ T cells treated with LDN27219 or fludarabine **for 24 h** were analyzed by qPCR (n = 3). **c**, ChIP-seq tracks at the *MFN2* locus comparing STAT pS727, H3K27ac signals (in reads per million) in SET-2 cells. **d**, ChIP-seq tracks at the *MTFR2* locus comparing STAT pS727, H3K27ac signals (in reads per million) in SET-2 cells. **e**, siRNA knockdown efficiency of *Mtfr2* in EL4 cells. Data are presented as mean ± SEM. ns, non-significant; *$p < 0.05$ by the unpaired Student's t-test
Extended Data Fig. 7	Single-cell landscape of *TPH1* expression and CD8$^+$ T cell subsets in non-small cell lung cancer.	**Extended Data Fig. 7**	**a**, UMAP visualization of major cell populations in non-small cell lung cancers (GSE189357) stratified by each sample and cell types. **b**, Bar charts showing TPH1 expression distribution and percentages of TPH1$^+$ cells in major cell types. **c**, Bar plot showing mean *TPH1* expression levels in each patient sample. **d**, UMAP visualization of five CD8$^+$ T cell subsets identified by unsupervised clustering. **e**, UMAP visualization of major cell populations in all cells and in cells stratified by treatment response group in non-small cell lung cancers before and after treatment with anti-PD-1+chemotherapy (GSE207422).

Supplementary Files

This is a list of supplementary files associated with this preprint. Click to download.

- ExtendedDataFig3.tif
- ExtendedDataFig2.tif
- ExtendedDataFig4.tif
- ExtendedDataFig5.tif
- ExtendedDataFig6.tif
- ExtendedDataFig7.tif
- ExtendedDataFig1.tif